A Lode-dependent Gurson model motivated by unit cell analyses

Lars Edvard Dæhli*, David Morin, Tore Børvik, Odd Sture Hopperstad

Structural Impact Laboratory (SIMLab), Department of Structural Engineering, Norwegian University of Science and Technology (NTNU), NO-7491 Trondheim, Norway

Abstract

In this study, the effects of including a dependency on the third deviatoric stress invariant in the void evolution equation of the Gurson model are examined using unit cell calculations and imperfection band analyses. Finite element analyses of a unit cell model are conducted to approximate the behaviour of the material microstructure. The unit cell was modelled as a cube made from an elastic-plastic matrix governed by J_2 flow theory with a spherical void located at the centre. The results of the unit cell calculations show a monotonic decrease in void growth when the stress state changes from generalized tension to generalized compression. To mimic the resulting evolution of the void volume fraction, an extension of the Gurson model based on the shear modification proposed by Nahshon and Hutchinson (2008) is proposed. This Lode-dependent void evolution term is further qualitatively assessed through comparisons with the unit cell simulations and through strain localization predictions using imperfection band analyses. The assessment demonstrates that the proposed modification of the void evolution equation is consistent with the evolution of the unit cell in the case of moderate and high stress triaxiality ratios. Furthermore, the imperfection band analyses exhibit a greater difference between the failure strain values in generalized tension and generalized compression using this Lode-dependent void evolution term compared to similar analyses that employ the original Gurson model or the shear-modified Gurson model. The Lode-dependent void evolution term thus renders the ductility predictions more consistent with previously reported studies based on unit cell calculations for the set of material parameters employed in this study.

Keywords: Unit cell; Lode dependency; Ductile failure; Gurson model; Strain localization

1. Introduction

The experiments performed by Bao and Wierzbicki (2004) indicated that stress triaxiality alone is not sufficient to quantify ductile fracture. This result has subsequently been corroborated by experiments under a variety of macroscopically imposed stress states using carefully designed tubular specimens (Barsoum and Faleskog, 2007; Haltom et al., 2013; Papasidero et al., 2015; Scales et al., 2016) or combinations of different test specimens (Beese et al., 2010; Faleskog and Barsoum, 2013). Although such experiments certainly prove that the deviatoric stress state affects the measured failure strain, they are difficult to use for quantifying inherent material ductility since the local loading paths generally deviate from the globally applied loading paths. The non-uniqueness of the ductile fracture locus under the application of non-proportional loading has been shown from both physical experiments (Basu and Benzerga, 2015) and from numerical analyses (Benzerga et al., 2012; Dæhli et al., 2016; Thomas et al., 2016). In general, it is extremely difficult to construct test specimens that yield exactly proportional loading paths in regions where failure initiates. Moreover, local stress measurements are not available from experimental data and must be acquired from numerical analyses. The stress measurements extracted from numerical simulations thus rely heavily on the adopted constitutive model. Some uncertainty regarding the predicted local loading path remains due to the hybrid experimental-numerical procedure, and whether physical experiments can be used to determine an intrinsic failure locus for a given material is questionable (Basu and Benzerga, 2015).

*Corresponding author
Email address: lars.e.dahli@ntnu.no (Lars Edvard Dæhli)

Nomenclature

Symbols

κ	Scaling function of Lode-dependent porosity term
ϕ, Φ	Microscopic and macroscopic yield function
$\boldsymbol{\sigma}, \boldsymbol{\Sigma}$	Microscopic and macroscopic stress tensor
σ_{eq}	Von Mises equivalent stress
σ_{h}	Hydrostatic stress
$\sigma_{\mathrm{I}}, \sigma_{\mathrm{II}}, \sigma_{\mathrm{III}}$	Principal stress components
σ_{M}	Matrix flow stress
σ_0	Initial yield stress
θ	Deviatoric angle
$\mathbf{C}^{\mathrm{t}}$	Material tangent stiffness
$\mathbf{d}, \mathbf{D}$	Microscopic and macroscopic rate-of-deformation
D_{eq}	Equivalent rate-of-deformation
E_{eq}	Equivalent strain
E, ν	Elastic material parameters
f	Void volume fraction/porosity
I_1	First principal invariant of the stress tensor
J_2	Second principal invariant of the deviatoric stress tensor
J_3	Third principal invariant of the deviatoric stress tensor
k_{s}	Parameter of Lode-dependent porosity term
$\mathbf{L}$	Velocity gradient
L	Lode parameter
$\mathbf{n}$	Imperfection band normal
$\mathbf{N}$	Nominal stress tensor
p	Matrix accumulated plastic strain
$\dot{\mathbf{q}}$	Velocity non-uniformity
Q, C	Isotropic hardening parameters
q_1, q_2	Tvergaard parameters
T	Stress triaxiality

Abbreviations

FE	Finite element
GC	Generalized compression
GS	Generalized shear
GT	Generalized tension
RVE	Representative volume element

The Gurson model (Gurson, 1977) is an extensively used porous plasticity model that incorporates material softening due to the growth of microscopic voids. This model is derived from an upper-bound plastic limit analysis of a hollow sphere with a rigid perfect-plastic matrix governed by J_2 flow theory. Consequently, there is only a single microstructural variable associated with the model, which is referred to as the void volume fraction or porosity. The void volume fraction is treated as an internal variable, and an evolution law is obtained from the condition of matrix incompressibility. However, the resulting porosity evolution law lacks the ability to predict the influence of the deviatoric stress state on the void growth. Numerical studies involving unit cell simulations (Zhang et al., 2001; Kim et al., 2004; Gao and Kim, 2006; Brünig et al., 2013) have shown that these effects of the deviatoric stress state are persistent at moderate and high stress triaxiality levels. Specifically, for a matrix material governed by J_2 flow theory, stress states corresponding to generalized tension are found to promote more rapid void growth, with the growth rate successively decreasing towards generalized compression loading. Moreover, the voids evolve into general ellipsoidal shapes that are dictated by the deviatoric stress state. Such arbitrary ellipsoidal void shapes are not consistent with the representative volume element (RVE) used in the Gurson model. Since void growth is of key importance for ductile failure in the case of moderate and high levels of stress triaxiality, the influence of the deviatoric stress state on the evolution of the void volume fraction is considered to be important in the context of porous plasticity modelling.

Several models that account for more general void shapes have been proposed over the past decades. In particular, Gologanu et al. (1993, 1994) included prolate and oblate void shapes, while Madou and Leblond (2012a,b) more recently derived a Gurson-type yield function for arbitrary ellipsoidal void shapes. Cao et al. (2015) recently presented a model for predicting ductile damage that accounts for void shape changes and void rotation, which are important components for modelling ductile fracture when the stress triaxiality is rather low. Shear-dominated loading states are known to result in localization and fracture due to void distortion and rotation, leading to linkage through a void-sheet mechanism (Korbel et al., 1984; Teirlinck et al., 1988). Experiments have shown that failure can occur at even lower strain levels under shear loading than under axisymmetric loading at higher stress triaxialities (Bao and Wierzbicki, 2004; Barsoum and Faleskog, 2007). Moreover, studies of strain localization based on bifurcation analysis or imperfection band analysis have revealed that failure loci typically have minima close to generalized shear states for low and moderate stress triaxialities. These findings are also substantiated by finite element simulations of unit cell models that specifically describe the voided imperfection band (Barsoum and Faleskog, 2011; Dunand and Mohr, 2014; Wong and Guo, 2015).

Although the more refined porous plasticity models are more appropriate since they inherently account for the effects associated with the void shape, they are also more complex from an implementation perspective. However, the inability of the original Gurson model to account for effects of the stress deviator, combined with the experimental observation that ductile fracture also occurs at low stress triaxialities, highlights the need for including some type of damage term driven by the deviatoric stress state that also operates under low stress triaxialities. A simple means to alleviate these issues regarding low stress triaxiality ratios could be to include a void nucleation term if the nucleation rate is sufficient to overcome the material hardening. However, after all the voids have been nucleated, a persisting low triaxiality stress state would either produce a rather constant porosity or, under negative triaxiality ratios, reduce the porosity. Unless a very large amount of void-nucleating particles are included in the analyses, this will not initiate ductile failure. This draws attention towards the extensions of

the Gurson model proposed by Nahshon and Hutchinson (2008) and Xue (2008) to account for damage due to void-induced shear softening. These shear-modified Gurson models employ shear damage functions that scale with an appropriate deviatoric stress state parameter. Furthermore, the scaling functions are symmetric with respect to generalized shear states, leaving no effect under generalized tension or generalized compression loading states. Zhou et al. (2014) proposed an alternative approach to include shear damage based on the work of Nahshon and Hutchinson (2008) and Xue (2008). Their approach is different in that they let the shear damage only affect the deviatoric part of the yield function, whereas in Nahshon and Hutchinson (2008) and Xue (2008) it is also coupled to the hydrostatic term. Additionally, Zhou et al. (2014) used a scaling function that enables damage accumulation under negative stress triaxialities based on the argument that failure also occurs for axisymmetric compressive loadings. The shear modifications proposed by Nahshon and Hutchinson (2008) and Xue (2008) have been shown to provide estimates for void growth that are too high in the case of high stress triaxialities. This was first noted by Nielsen and Tvergaard (2010) who further proposed a linear scaling of the shear damage term presented by Nahshon and Hutchinson (2008) to maintain the predictions of the Gurson model under high stress triaxialities.

Conducting physical experiments that enable full control of the obtained loading path is generally impossible. Although test specimens exist that offer nearly proportional loading, there are currently no experimental procedures that can be used to vary the deviatoric stress state while keeping the stress triaxiality ratio fixed. Given this inherent limitation of physical material tests, in the current paper, we motivate the modification of the Gurson model using numerical unit cell analyses of approximate material microstructures where the stress state is fully controlled by the user. Specifically, we intend to address the effects of the Lode parameter or the deviatoric angle on the void growth. Although we aspire to include a physically motivated scaling of the void growth in terms of the deviatoric angle through comparisons with microstructural finite element simulations, we have restricted our attention to a highly idealized RVE consisting of an initial uniform distribution of spherical voids. Thus, we do not consider general void shapes using more advanced porous plasticity models, such as Madou and Leblond (2012a,b) and Cao et al. (2015); rather, we intend to address the issue through a heuristic extension of the Gurson model (Gurson, 1977) consistent with the work of Nahshon and Hutchinson (2008). Furthermore, the unit cell model is restricted to prescribe normal stress components, and we consequently exclude the effects of void rotation and shearing, which are of key importance for ductile fracture under low stress triaxialities. Recently, Vadillo et al. (2016) used a different approach to incorporate the effects of the third deviatoric invariant into the Gurson model in the range of high stress triaxialities. Their model is based on specifying the material parameters q_i entering the Gurson-Tvergaard model (Gurson, 1977; Tvergaard, 1981, 1982) directly as functions of the Lode parameter.

The unit cell analyses in the following are treated as the true material behaviour and serve as the experimental basis for our study. However, in the general case, the unit cell model used herein can only be considered an idealization of the real material behaviour. With these remarks in mind, the primary objective of this study is to include a void evolution equation in the Gurson yield criterion that conforms with unit cell calculations. Moreover, we emphasize that the Lode extension proposed herein is based on observations that pertain to moderate and high levels of stress triaxiality. Such stress states can be obtained in many structural applications since structures often contain regions of very constrained deformation; even for thin-walled structures, buckling may lead to local zones of high hydrostatic tension. Regardless, this model should be interpreted as a potential remedy for the deficiency associated with the lack of Lode dependency in the original Gurson model. The motivation is to propose a simple heuristic extension that does not introduce additional complexities in the numerical implementation compared to the original model. We note that ductile failure under low stress triaxiality is observed to be largely associated with void rotation and material shearing. Consequently, this model is not expected to yield a realistic prediction under such circumstances. However, the predictions will not be impaired compared with the original Gurson model, and the model inherits the features of the shear-modified Gurson model (Nahshon and Hutchinson, 2008) under shear-dominated loadings.

In Section 2, we present the necessary theoretical background for this study. The unit cell model and some relevant results from the numerical unit cell analyses are highlighted in Section 3. Next, the key findings of the unit cell study, which motivate the current modification of the Gurson model, are presented in Section 4 along with the proposed modification and the previous extension by Nahshon and Hutchinson (2008). Section 5 is dedicated to assessing the modified void evolution equation using unit cell simulations and ductility predictions based on imperfection band analyses. Some concluding remarks are provided in Section 6.

2. Theoretical preliminaries

2.1. Stress state parameters

An arbitrary stress state, denoted P in Figure 1, can be expressed in the principal stress space with the ordered principal stress components written as the sum of a deviatoric part and a hydrostatic part according to

$$\sigma_{\mathrm{I}} = \frac{2}{3}\sigma_{\mathrm{eq}}\cos(\theta) + \sigma_{\mathrm{h}} \tag{1a}$$

$$\sigma_{\mathrm{II}} = \frac{2}{3}\sigma_{\mathrm{eq}}\cos\left(\theta - \frac{2\pi}{3}\right) + \sigma_{\mathrm{h}} \tag{1b}$$

$$\sigma_{\mathrm{III}} = \frac{2}{3}\sigma_{\mathrm{eq}}\cos\left(\theta + \frac{2\pi}{3}\right) + \sigma_{\mathrm{h}} \tag{1c}$$

The stress components are ordered as $\sigma_{\mathrm{I}} \geq \sigma_{\mathrm{II}} \geq \sigma_{\mathrm{III}}$, and the deviatoric angle θ is then confined to the interval $0° \leq \theta \leq 60°$. Furthermore, $\sigma_{\mathrm{eq}} = \sqrt{3J_2}$ is the von Mises equivalent stress and $\sigma_{\mathrm{h}} = I_1/3$ is the hydrostatic stress, where the second principal deviatoric stress invariant and the first principal stress invariant are denoted J_2 and I_1, respectively. We refer to Figure 1a for an illustration of the stress state P in the principal stress space and to Figure 1b for a corresponding illustration in the deviatoric stress plane. Note that the deviatoric angle is the angle between the direction of the stress point and a projected base vector along the σ_{I}-axis in the deviatoric plane.

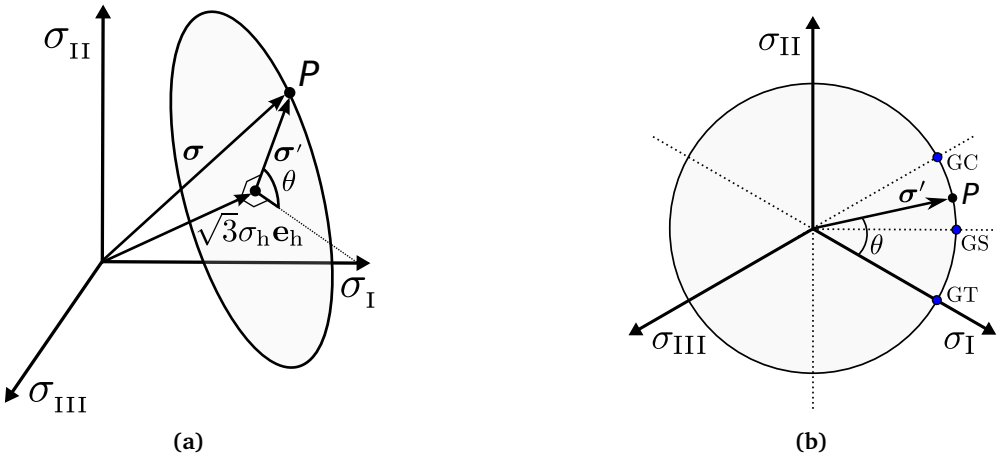

Figure 1: Illustration of a stress point P in (a) the principal stress space and (b) the deviatoric stress plane. The deviatoric and hydrostatic parts of the stress vector are indicated in the figure and the hydrostatic axis is denoted by $\mathbf{e}_{\mathrm{h}}$. The depicted ellipse, which is a circle in the deviatoric plane, describes stress points with the same stress triaxiality ratio T. *GT*, *GS*, and *GC* refer to generalized tension, shear and compression, respectively.

Throughout this study, we will use the stress triaxiality T, the deviatoric angle θ, and the Lode parameter L to describe the stress state. The stress triaxiality is defined from the hydrostatic stress σ_{h} and the von Mises equivalent stress σ_{eq} in the form

$$T = \frac{\sigma_{\mathrm{h}}}{\sigma_{\mathrm{eq}}} = \frac{I_1}{3\sqrt{3J_2}} \tag{2}$$

To describe the deviatoric stress state, the Lode parameter is defined as a ratio between the principal stress components given by

$$L = \frac{2\sigma_{\mathrm{II}} - \sigma_{\mathrm{I}} - \sigma_{\mathrm{III}}}{\sigma_{\mathrm{I}} - \sigma_{\mathrm{III}}} \tag{3}$$

A relation between the Lode parameter and the third deviatoric stress invariant $J_3 = \det(\boldsymbol{\sigma}')$ is provided by the

following two equations

$$L = \sqrt{3}\tan\left(\theta - \frac{\pi}{6}\right) \tag{4a}$$

$$\cos(3\theta) = \frac{27}{2}\frac{J_3}{\sigma_{\text{eq}}^3} \tag{4b}$$

From the definition of the Lode parameter, it follows that $L = -1$, 0, and 1 correspond to $\theta = 0°$, 30°, and 60°, respectively. Additionally, both the Lode parameter and the deviatoric angle are exclusively linked to the deviatoric stress state and are thus independent of the hydrostatic stress. In this paper, we will utilize both L and $\cos(3\theta)$ and we note that they are related through

$$\cos(3\theta) = -\sin\left(3\arctan\left(\frac{L}{\sqrt{3}}\right)\right) \tag{5}$$

We also note that Lode parameters $L = -1$ ($\theta = 0°$), 0 ($\theta = 30°$), and 1 ($\theta = 60°$) represent states of generalized tension, shear, and compression, respectively, which will often be referred to in the following. In terms of $\cos(3\theta)$, these stress states correspond to 1, 0, and -1.

2.2. Matrix material

A corotational framework is used to formulate the constitutive relations of the matrix material. The corotated stress tensor $\hat{\boldsymbol{\sigma}}$ and the corotated rate-of-deformation tensor $\hat{\mathbf{d}}$ read

$$\hat{\boldsymbol{\sigma}} = \mathbf{R}^T \cdot \boldsymbol{\sigma} \cdot \mathbf{R} \tag{6a}$$

$$\hat{\mathbf{d}} = \mathbf{R}^T \cdot \mathbf{d} \cdot \mathbf{R} \tag{6b}$$

where $\boldsymbol{\sigma}$ and $\mathbf{d}$ are the Cauchy stress tensor and the rate-of-deformation tensor, respectively. Transformation between the local material basis and the global basis is governed by the orthogonal rotation tensor $\mathbf{R}$. The implicit finite element (FE) solver ABAQUS/Standard employs the Jaumann stress rate, and the local material basis is then updated according to $\dot{\mathbf{R}} = \mathbf{w} \cdot \mathbf{R}$, where $\mathbf{w}$ denotes the material spin. The corotated rate-of-deformation tensor is additively split into an elastic part and a plastic part such that

$$\hat{\mathbf{d}} = \hat{\mathbf{d}}^{\text{e}} + \hat{\mathbf{d}}^{\text{p}} \tag{7}$$

The rate form of the generalized Hooke's law is used to account for the elastic response. Hence, the corotated stress rate tensor $\hat{\boldsymbol{\sigma}}$ is linked to the corotated elastic rate-of-deformation tensor $\hat{\mathbf{d}}^{\text{e}}$ through

$$\hat{\boldsymbol{\sigma}} = \frac{E}{1+\nu}\hat{\mathbf{d}}^{\prime\text{e}} + \frac{E}{3(1-2\nu)}\text{tr}(\hat{\mathbf{d}}^{\text{e}})\mathbf{1} \tag{8}$$

where $\hat{\mathbf{d}}^{\prime\text{e}}$ and $\text{tr}(\hat{\mathbf{d}}^{\text{e}})$ are the deviatoric and volumetric parts of $\hat{\mathbf{d}}^{\text{e}}$, respectively, and $\mathbf{1}$ is the second-order identity tensor. The selected values for the elastic modulus E and Poisson's ratio ν are listed in Table 1. The plastic response of the matrix material is described by the rate-independent J_2 flow theory with an associated flow rule. Work hardening is governed by the Voce rule

$$\sigma_{\text{M}} = \sigma_0 + Q(1 - \exp(-Cp)) \tag{9}$$

where σ_{M} is the flow stress, σ_0 denotes the initial yield stress, Q and C are material constants, and p is the accumulated plastic strain. The material parameters used herein are listed in Table 1. We note that these parameters are generic, but representative for aluminium alloys exhibiting low work hardening. The equivalent plastic strain rate is taken to be power conjugate to the matrix flow stress, and the accumulated plastic strain is

accordingly evaluated from

$$p = \int_0^t \dot{p}\,\mathrm{d}\bar{t} = \int_0^t \frac{\hat{\boldsymbol{\sigma}} : \hat{\mathbf{d}}^{\mathrm{p}}}{\sigma_{\mathrm{M}}}\,\mathrm{d}\bar{t} \tag{10}$$

Table 1: Generic material parameters used for the matrix material.

E [GPa]	ν	σ_0 [MPa]	Q [MPa]	C
70	0.3	100	100	10

2.3. Porous plasticity model

The Gurson model (Gurson, 1977) with the modification proposed by Tvergaard (1981, 1982) is used to govern the homogenized material response throughout this study. Consistent with the matrix constitutive model, the porous plasticity model is formulated in a corotational basis to ensure material objectivity. The yield function reads

$$\Phi\left(\hat{\boldsymbol{\Sigma}}, \sigma_{\mathrm{M}}, f\right) = \left(\frac{\Sigma_{\mathrm{eq}}}{\sigma_{\mathrm{M}}}\right)^2 + 2q_1 f \cosh\left(\frac{3}{2}q_2\frac{\Sigma_{\mathrm{h}}}{\sigma_{\mathrm{M}}}\right) - 1 - (q_1 f)^2 \leq 0 \tag{11}$$

where $\hat{\boldsymbol{\Sigma}}$ is the corotated macroscopic stress tensor, Σ_{eq} denotes the macroscopic von Mises equivalent stress, Σ_{h} is the macroscopic hydrostatic stress, and σ_{M} is the matrix flow stress, which is governed by Equation (9). The model parameters q_i were introduced by Tvergaard (1981, 1982). The volume fraction of microvoids is represented by the scalar quantity f, which is referred to as the void volume fraction or porosity. We note that the evolution of the porosity is the main focus of this study.

The associated flow rule is adopted herein, and the macroscopic plastic rate-of-deformation tensor is given by

$$\hat{\mathbf{D}}^{\mathrm{p}} = \dot{\Lambda}\frac{\partial \Phi}{\partial \hat{\boldsymbol{\Sigma}}} \tag{12}$$

where $\dot{\Lambda} \geq 0$ is the plastic multiplier. The equivalence in plastic power provides a relation for the equivalent plastic strain rate of the form

$$\hat{\boldsymbol{\Sigma}} : \hat{\mathbf{D}}^{\mathrm{p}} = (1-f)\,\sigma_{\mathrm{M}}\dot{p} \quad \Rightarrow \quad \dot{p} = \frac{\hat{\boldsymbol{\Sigma}} : \hat{\mathbf{D}}^{\mathrm{p}}}{(1-f)\,\sigma_{\mathrm{M}}} \tag{13}$$

The loading-unloading conditions of the rate-independent porous plasticity formulation reads

$$\Phi \leq 0, \quad \dot{\Lambda} \geq 0, \quad \Phi\dot{\Lambda} = 0 \tag{14}$$

In the current study, we intend to investigate the influence of the Lode parameter on the void evolution. Starting from the shear-modified Gurson model (Nahshon and Hutchinson, 2008), we use an extra void evolution term such that the total rate of porosity change is written in the general form

$$\dot{f} = \dot{f}_{\mathrm{g}} + \dot{f}_{\mathrm{s}} \tag{15}$$

In this formulation, $\dot{f}_{\mathrm{g}}$ denotes the usual void growth term resulting from matrix incompressibility (Gurson, 1977), and $\dot{f}_{\mathrm{s}}$ is an additional term that incorporates the effects of the deviatoric stress state. As noted by Nahshon and Hutchinson (2008), the introduction of $\dot{f}_{\mathrm{s}}$ violates the mass balance of the RVE, and the porosity should in this case be treated as a damage parameter rather than the actual void volume fraction. However, we will still refer to f as the porosity or void volume fraction in the following since we employ this term to enhance the correlation with the void evolution from unit cell simulations.

Two different expressions for $\dot{f}_{\mathrm{s}}$ will be used herein. The first pertains to the shear-modified damage term of Nahshon and Hutchinson (2008), while the second is a slight modification of the same term which we will

present in Section 4.2. However, we note that in the present context, the extra term $\dot{f}_{\mathrm{s}}$ is motivated by the Lode dependency of the void growth as observed in unit cell calculations and should be considered as a void distortion term rather than as a shear damage term. Both relations for $\dot{f}_{\mathrm{s}}$ may be expressed quite generally as

$$\dot{f}_{\mathrm{s}} = k_{\mathrm{s}} f \kappa(\theta) D^{\mathrm{p}}_{\mathrm{eq}} \tag{16}$$

where we have introduced the equivalent deviatoric plastic strain rate $D^{\mathrm{p}}_{\mathrm{eq}}$ by

$$D^{\mathrm{p}}_{\mathrm{eq}} = \frac{\hat{\boldsymbol{\Sigma}}' : \hat{\mathbf{D}}^{\mathrm{p}}}{\Sigma_{\mathrm{eq}}} \tag{17}$$

Additionally, $\hat{\boldsymbol{\Sigma}}'$ denotes the deviatoric part of the corotated macroscopic stress tensor, k_{s} is a constant factor, and $\kappa(\theta)$ expresses some function of the deviatoric angle θ, which is considered in more detail in Section 4.2. We note that $\dot{f}_{\mathrm{s}}$ can be written in terms of the plastic multiplier $\dot{\Lambda}$ through the associated flow rule given in Equation (12). The void evolution law in Equation (15) is then written as

$$\dot{f} = \left((1-f)\,\mathrm{tr}\left(\frac{\partial \Phi}{\partial \hat{\boldsymbol{\Sigma}}} \right) + \frac{k_{\mathrm{s}} f \kappa(\theta)}{\Sigma_{\mathrm{eq}}} \hat{\boldsymbol{\Sigma}}' : \frac{\partial \Phi}{\partial \hat{\boldsymbol{\Sigma}}} \right) \dot{\Lambda} \tag{18}$$

3. Observations from unit cell simulations

3.1. Numerical setup

We employ an RVE consisting of a cube with a spherical centred void, as shown in Figure 2a. Thus, we approximate the material microstructure by a uniform distribution of equally spaced spherical voids embedded in a plastically incompressible isotropic elasto-plastic matrix defined by the constitutive model outlined in Section 2.2. The RVE defines the unit cell, which is modelled in the finite element (FE) software ABAQUS/Standard (Abaqus, 2013). We further assume that the unit cell orientation coincides with the principal stress directions; thus, only normal stress components are assigned globally to the unit cell model. Consequently, we can exploit the symmetries of the governing problem to model only one-eighth of the RVE for computational efficiency. This excludes situations in which the void is rotating due to macroscopic shearing, which is of key importance under low stress triaxiality conditions where failure presumably occurs through a void-sheet mechanism. We have consequently restricted the majority of the simulations to moderate and high levels of stress triaxiality, with the exception of one set of calculations under zero triaxiality including a particle. Note that this study is primarily concerned with the void growth stage, and that the last stage of ductile failure involving void coalescence is not specifically addressed herein.

The unit cell boundaries are constrained to remain straight to enforce periodicity. The void is free of traction forces, but otherwise free to deform. The initial unit cell geometry is defined by the edge lengths $L_1 = L_2 = L_3 = 2\bar{L}$, where $\bar{L}$ is the dimension of the edges employed in the $1/8$ model. The spherical void has a radius $R_1 = R_2 = R_3 = \bar{R}$, and the initial void volume fraction is given by

$$f_0 = \frac{V_{\mathrm{v}}}{V_{\mathrm{RVE}}} = \frac{\pi}{6} \left(\frac{\bar{R}}{\bar{L}} \right)^3 \tag{19}$$

where V_{v} and V_{RVE} denote the volumes of the void and the RVE, respectively. An initial porosity of $f_0 = 0.005$ was utilized in all calculations. The chosen void volume fraction is considered to be representative for the content of the primary particles in some typical aluminium alloys (Westermann et al., 2014).

We use nonlinear kinematical constraints on the nodal displacements of the unit cell to impose displacements that maintain the stress ratios at prescribed values. This approach provides the ability to control the loading path by imposing values of the stress triaxiality ratio T and the Lode parameter L. These were implemented by enforcing work equivalence in a fictitious node, and the degrees of freedom of that node are used to constrain the unit cell boundaries by the use of a multi-point constraint (MPC) user subroutine. We will not outline the method

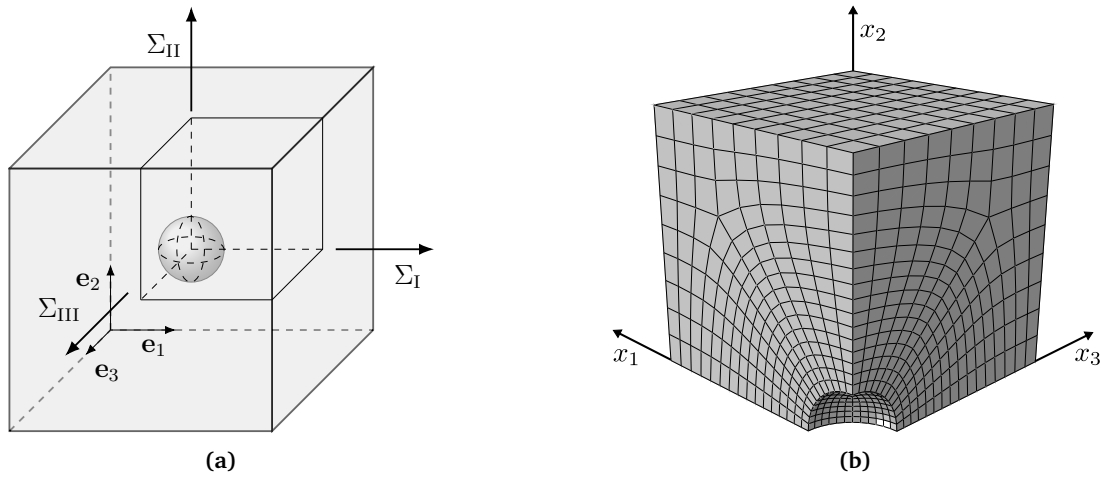

(a) **(b)**

Figure 2: Illustration of the unit cell model showing (a) the adopted RVE and (b) the spatially discretized FE model.

here since it is detailed in other studies (see e.g. Faleskog et al. (1998), Kim et al. (2004), Cheng and Guo (2007), Liu et al. (2016), or Dæhli et al. (2017a)).

The unit cell model consists of nearly 2000 linear 8-node solid elements (C3D8 in ABAQUS). The spatial discretization of the FE model is shown in Figure 2b. We note that the C3D8 elements are selectively integrated by default to reduce susceptibility towards volumetric locking, which could represent a numerical problem for the nearly incompressible matrix behaviour displayed under predominant plastic loading. We conducted a preliminary mesh convergence study to ensure a converged unit cell response; however, the details of that study are omitted here for brevity.

We use an equivalent macroscopic strain measure to compare the macroscopic stress and the void volume fraction under different loading conditions. The equivalent strain is calculated from

$$E_{\mathrm{eq}} = \sqrt{\frac{2}{3}\mathbf{E}' : \mathbf{E}'} \tag{20}$$

where $\mathbf{E}'$ denotes the deviatoric macroscopic strain. Due to the symmetry boundary conditions used to enforce periodicity of the reduced unit cell model, there are no macroscopic shear strain components on the unit cell. Thus, we calculate the normal logarithmic strain components from

$$E_i = \ln\left(\frac{l_i}{L_i}\right), \quad i = 1,2,3 \text{ (no sum over i)} \tag{21}$$

where L_i and l_i refer to lengths of the unit cell in the initial and current configurations, respectively.

3.2. Macroscopic unit cell response

We performed unit cell simulations with an initial void under loading states governed by stress triaxiality ratios $T = 1/\sqrt{3}, 2/3, 1, 5/3$, and 3. The entire range of deviatoric stress states was covered, and we specifically imposed the five different Lode parameters $L = -1, -1/2, 0, 1/2$, and 1. The unit cell simulations were terminated when the unit cell response had softened to an equivalent stress level of $\Sigma_{\mathrm{eq}} = 0.8\Sigma_{\mathrm{eq}}^{\mathrm{max}}$ or when excessive deformation of the unit cell was obtained in the simulation. The global strain increments were stepped down in the elastic loading domain to capture the onset of plastic yielding and then gradually increased to a final step size in the plastic loading domain. This led to approximately 100 time increments during the loading stage. Selected response curves from all the unit cell calculations are plotted in Figure 3.

Figures 3a and 3b present simulation data for the normalized macroscopic stress and the void volume fraction, respectively, as functions of the equivalent strain defined in Equation (20). The equivalent macroscopic stress

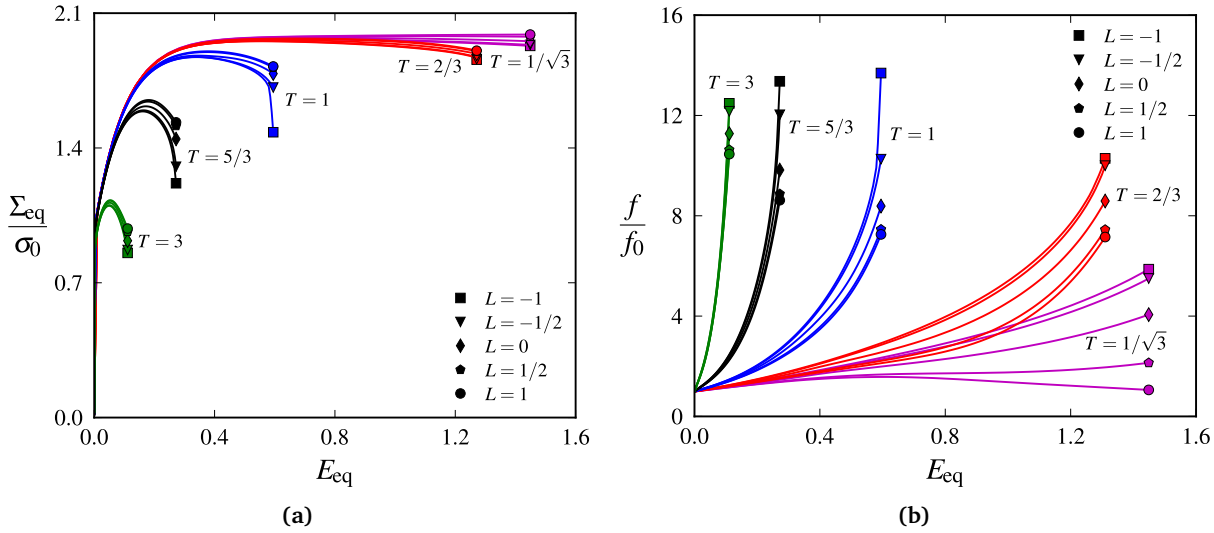

Figure 3: Numerical results from the unit cell analyses. Figure (a) shows the normalized equivalent stress as a function of the equivalent strain. Figure (b) shows the normalized void content as a function of the equivalent strain.

curves shown in Figure 3a demonstrate pronounced softening of the unit cell under high stress triaxialities. This is caused by the rapid expansion of the void under predominant hydrostatic tensile loading. Although this effect somewhat diminishes when the stress triaxiality decreases, we still infer that the overall response of the unit cell softens for rather large strains. An exception corresponds to loading under $T = 1/\sqrt{3}$ and $L = 1$, for which the void tends to collapse and thus provides a saturated stress level. From the void growth curves shown in Figure 3b, we observe an influence of the Lode parameter on the unit cell response. This is particularly pronounced for the lower stress triaxialities employed in this study, whereas the effect is diminished for high stress triaxiality ratios. All stress triaxialities have more prominent void growth under generalized tension $L = -1$, with a successively decreasing void growth rate for increasing Lode parameters. The void growth rate reaches a minimum as the imposed stress state corresponds to generalized compression $L = 1$. This trend has been reported in several unit cell studies conducted over the past two decades; for example, see Zhang et al. (2001), Kim et al. (2004), and Gao and Kim (2006). We note that for generalized compression, the void collapses for a stress triaxiality level of $T = 1/\sqrt{3}$ with the given matrix hardening parameters. This means that we are already pushing the limit of the Gurson-type models in this range of stress triaxiality when compared to unit cell simulations since such porous plasticity models will predict an increase in porosity for all positive stress triaxiality ratios.

The dependency of the unit cell response, and particularly the void growth, on the Lode parameter can be attributed to the evolution of the void shape. Figure 4 displays the void edges that connect the void principal axes. The void edges are plotted both in the initial unit cell configuration (dotted lines) and in the configuration corresponding to the onset of macroscopic softening. Void shapes for the Lode parameters $L = -1, 0$, and 1 are shown for the stress triaxialities $T = 2/3, 5/3$ and 3. The red curves correspond to the x_1x_2-plane, the blue curves correspond to the x_1x_3-plane, and the green curves correspond to the x_2x_3-plane. The displayed results clearly demonstrate that the voids evolve into a prolate form under generalized tension and an oblate form under generalized compression prior to the onset of localized plastic deformation inside the unit cell. This is a well-known effect, which has already been demonstrated by Budiansky et al. (1982) in an analytical study of void growth in non-linear viscous solids. Similar observations have subsequently been made using unit cell model calculations (see e.g. Zhang et al. (2001); Gao and Kim (2006); Brünig et al. (2013)). The effect of the Lode parameter on the void shape evolution is more evident when the stress triaxiality ratio is lowered, which is easily recognized from the results corresponding to $T = 2/3$ in Figure 4. As the stress triaxiality ratio increases, the Lode dependency of the void evolution fades out. However, note that even at the rather high triaxiality level $T = 5/3$, there is still a quite pronounced effect of the deviatoric loading state. When the stress triaxiality corresponds to $T = 3$, Figure 4 does not display any apparent differences between the void edges in either of the x_ix_j-planes,

which means that the void shape is rather spherical. This is also substantiated by the results shown in Figure 3b, where the void volume fraction curves for $T = 3$ are practically coinciding. However, note that due to the rather steep slope of these porosity-strain curves, some influence of the Lode parameter still persists when the void volume fraction levels are compared for different Lode parameters at the same equivalent strain level. We will address this more carefully in Section 4.

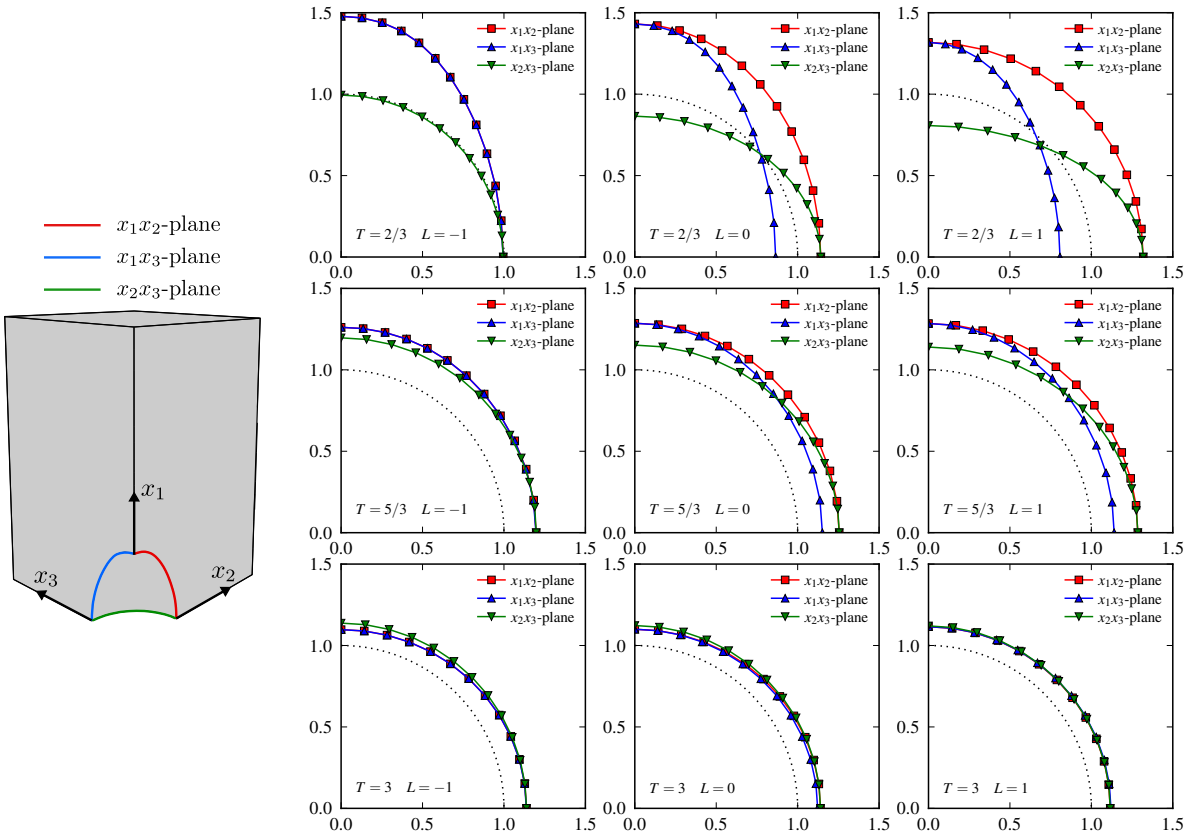

Figure 4: Plots of the void edges in the x_ix_j-planes in terms of normalized principal void radii. The black dotted curves represent the initial spherical void, whereas the red (□), blue (△), and green (▽) coloured solid lines correspond to the x_1x_2-plane, x_1x_3-plane, and x_2x_3-plane, respectively. The deformed void shapes are taken at the point of peak equivalent stress.

In conjunction with the porous plasticity models typically used at the homogenized material level, the effect of the Lode parameter on void growth is rather important. The Gurson model (Gurson, 1977), with the modifications due to Tvergaard (1981, 1982), is derived on the basis of spherical voids. This precludes any effect of the Lode parameter. More refined Gurson-type models have been proposed in the literature (Gologanu et al., 1993; Madou and Leblond, 2012a,b; Cao et al., 2015), in which the voids have more general shapes. Such descriptions have the advantage of intrinsically accounting for the effect of the Lode parameter due to the non-spherical assumption of the void shape. Additionally, these enhanced porous plasticity models are considered to be very important in the context of modelling ductile failure under low stress triaxialities since both void shape changes and void rotation are of key importance to fracture under shear-dominated stress states. However, it appears that the Gurson model with the q_i modification (Tvergaard, 1981, 1982) is still the most used porous plasticity model. This is primarily related to its simpler formulation and implementation in FE solvers. However, simpler extensions of the Gurson framework, in which the void growth equation is augmented by a shear damage term, are also available (Nahshon and Hutchinson, 2008; Xue, 2008). Since these models do not introduce any considerable complexity into the constitutive equations, they are appealing from an implementation and usage perspective. A modification of the

Gurson model that yields the ability to account for the tendencies observed in the unit cell simulations is then considered to be important for enhancing the predictive capabilities of the porous plasticity model.

4. Void growth relationships

In the following, we will address the main aspects of void growth as observed from unit cell analyses. We will briefly review the shear damage term proposed by Nahshon and Hutchinson (2008). Furthermore, we will propose a modification of this shear damage term to obtain better correspondence to the unit cell calculations.

4.1. Qualitative aspects of void growth

The unit cell analyses summarized in Section 3.2 suggest that the void growth is dependent on the deviatoric stress state in such a way that states of generalized tension generally promote the highest void growth rate. Although the extension of the Gurson model by Nahshon and Hutchinson (2008) incorporates the effects of the Lode parameter on the porosity evolution, this extension is not consistent with the observations made from the unit cell analyses in the current study. In the following, we will direct the attention towards an extension of the Gurson model that follows the work of Nahshon and Hutchinson (2008), but which incorporates a different scaling with respect to the deviatoric angle.

Figures 5a, 5c, and 5e show the normalized void volume fraction as a function of the equivalent strain for $T = 1/\sqrt{3}$, 2/3, and 3, respectively. In these figures, the normalized void volume fraction at three different levels of equivalent strain has been highlighted using red, blue, and black dots. The logarithm of the normalized void volume fraction at the same levels of equivalent strain is then shown with corresponding colours in Figures 5b, 5d, and 5f as a function of $\cos(3\theta)$. Note that $\cos(3\theta) = 1$ and $L = -1$ correspond to generalized tension, whereas $\cos(3\theta) = -1$ and $L = 1$ correspond to generalized compression. In general, these parameters are related through the non-linear expression presented in Equation (5). The purpose of these figures is to demonstrate that, in the void growth phase, the logarithm of the porosity is increasing in a nearly linear manner with the parameter $\cos(3\theta)$ used in the shear damage term by Nahshon and Hutchinson (2008). Moreover, these plots suggest that an appropriate scaling of the porosity rate might take the form $\dot{f}_s \sim f(1 + \cos(3\theta))$, which sets the agenda for Section 4.2.

An important issue should be addressed at this point. The unit cell results presented thus far only show how the evolution of the void volume fraction scales with the deviatoric loading conditions under moderate and high levels of stress triaxiality. This range of stress states was chosen because the unit cell model does not include the effects of void shearing and rotation, which are important for the ductile failure process under low stress triaxialities. The basis for the current extension of the Gurson model is to propose a correction for the inability to display Lode effects related to void evolution, but the governing mechanism is still void growth and not void shearing and rotation. Lower stress triaxiality ratios are thus not expected to fit the scope of this model and are consequently not addressed in any detail herein. However, the shear modification proposed by Nahshon and Hutchinson (2008) was mainly motivated by the occurrence of ductile failure also under shear-dominated loadings. Specifically, they considered a state of pure shear in which the void growth in the original Gurson model (see the first term in Equation (18)) reduces to zero. This renders the void volume fraction constant and will not promote ductile failure using the Gurson model. Thus, Nahshon and Hutchinson (2008) extended the usual void growth equation of the Gurson model to incorporate shear damage. Their term is symmetric with respect to generalized shear states $L = 0$, and it reduces to zero under purely axisymmetric stress states. However, they specifically state in their paper that no attempt was made to distinguish between axisymmetric states of $L = -1$ and $L = 1$. This choice was justified by the lack of experimental data allowing discriminating such stress states under shear-dominated loadings and from the observation that ductile failure under low stress triaxiality occurs due to a void-sheeting mechanism. In fact, such experimental studies are extremely difficult to conduct, and they would additionally require advanced imaging techniques to quantify the damage evolution *in situ*. In this paper, we have rather used an idealized representation of the microstructure to evaluate the void growth using unit cell simulations. In the following, these results are treated as experimental data from an idealized model material.

In situations where the hydrostatic tensile stress is low or even vanishing, the unit cell calculations will not lead to void growth. The initial void instead collapses, leaving a zero porosity with a unit cell response corresponding

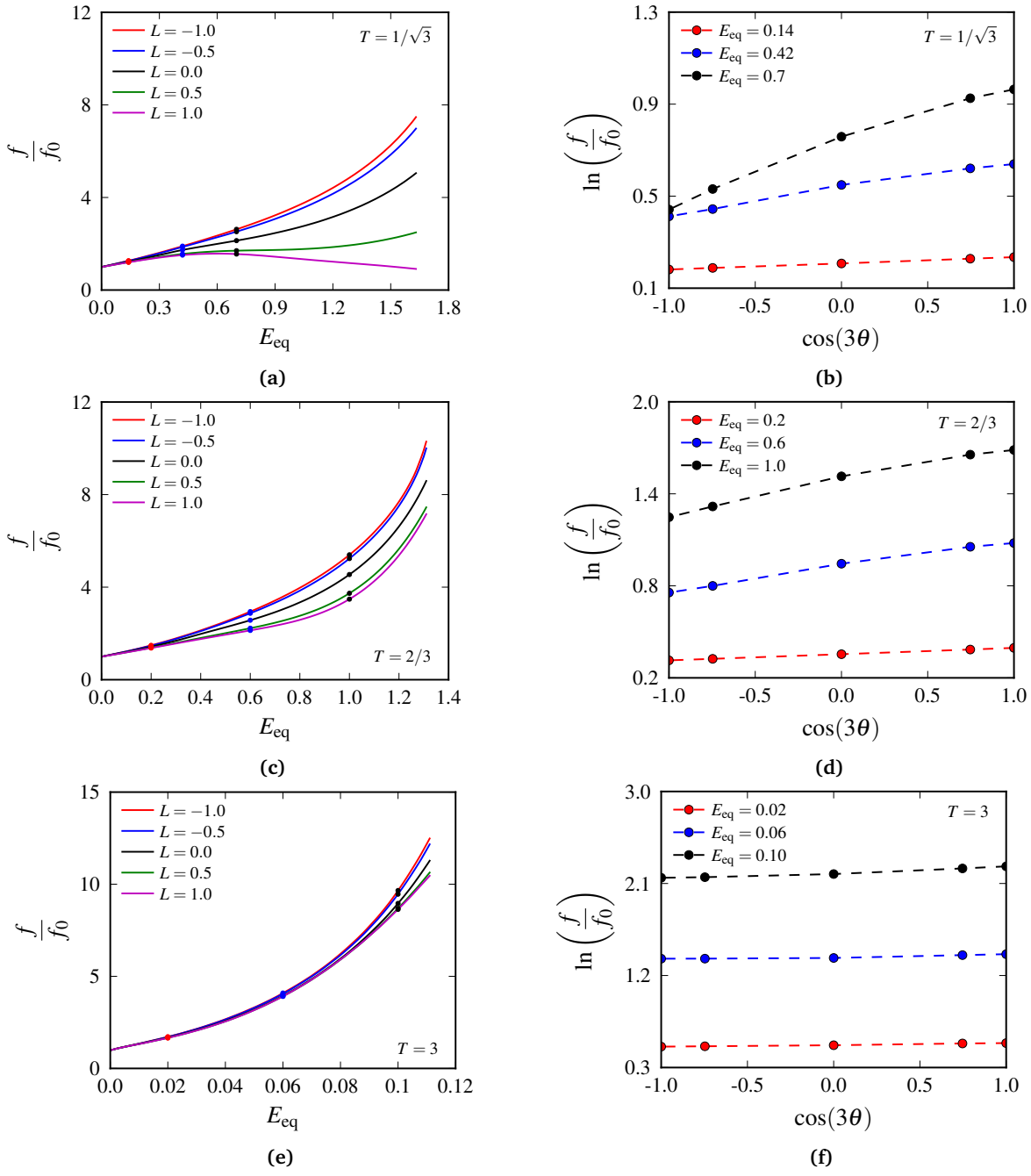

Figure 5: Numerical results from the unit cell analyses that show the scaling of the void evolution with the Lode parameter L or the deviatoric angle θ. Figures (a), (c), and (e) show the normalized porosity as a function of the equivalent strain for various Lode parameters and triaxialities of $T = 1/\sqrt{3}$, $2/3$, and 3, respectively. Figures (b), (d), and (f) show the logarithm of the normalized porosity as a function of $\cos(3\theta)$ for given levels of equivalent strain with imposed triaxialities of $T = 1/\sqrt{3}$, $2/3$, and 3, respectively.

to that of a material block without any defects. This is readily inferred by considering the evolution of the porosity for $T = 1/\sqrt{3}$ and $L = 1$ in Figure 3b, where the porosity rate becomes negative for rather large strains. Thus, we note that this already hints at the limitations of the porous plasticity model in terms of validity compared to unit

cell calculations. However, metal alloys often contain particles from which the voids nucleate. These particles are of great importance in the current context since they might prevent void closure and thus promote void growth. To examine this aspect, we performed a few additional unit cell simulations with a particle embedded in the matrix rather than a void. We modelled the particle as a rigid sphere, which is an approximation that can be justified for the typically harder particles in aluminium alloys. Furthermore, we assumed that there is no cohesive surface on the matrix-particle interface, and we employed frictionless hard contact between the matrix and the particle. This effectively excludes the possibility of void collapse, and we obtain some void growth even under zero triaxiality conditions.

Figure 6 presents numerical data for the unit cell with the rigid inclusion subjected to a stress triaxiality of $T = 0$. The key observation from the displayed void growth curves is that the generalized tension states still promote faster void growth. However, the void growth is more or less coinciding for the Lode parameters $L = 0$, 0.5, and 1. This result is not consistent with the linear trend observed for the higher triaxiality when the void volume fractions at given strain levels are plotted against the parameter $\cos(3\theta)$. Despite this non-conformity, we find the difference in the curves shown in Figure 6b sufficiently small to justify the use of a linear term. This is also motivated by the desire to use exactly the same model formulation for arbitrary stress states without having to make the deviatoric scaling function $\kappa(\theta)$ in Equation (18) a function of the stress triaxiality ratio.

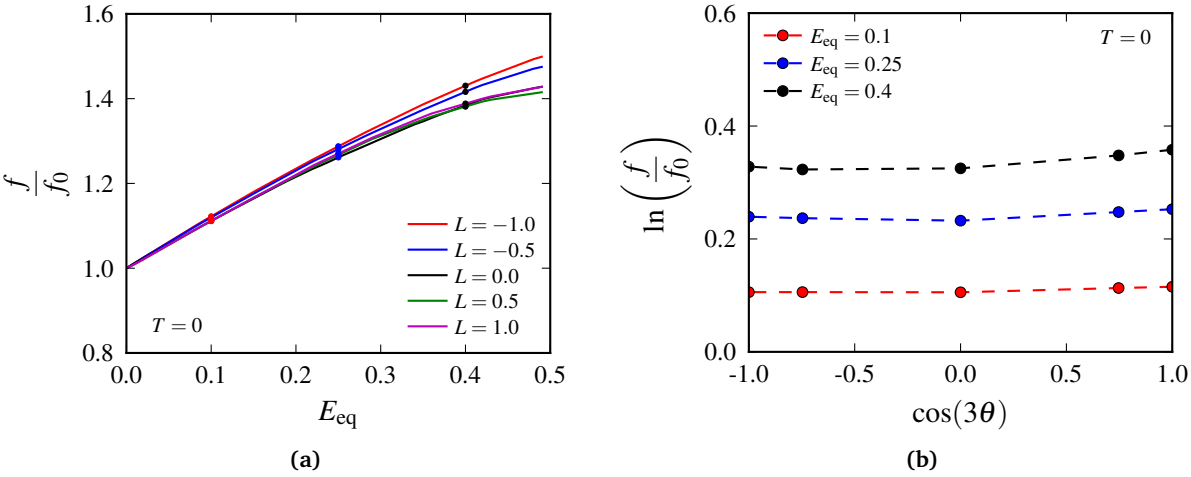

Figure 6: Numerical results from the unit cell analyses with a rigid particle. Figure (a) shows the normalized porosity as a function of the equivalent strain for various Lode parameters at triaxiality $T = 0$. Figure (b) shows the logarithm of the normalized porosity as a function of $\cos(3\theta)$ for given levels of equivalent strain with imposed triaxiality $T = 0$.

4.2. Modified void evolution term

Nahshon and Hutchinson (2008) used a deviatoric scaling function of the form

$$\kappa(\theta) = 1 - \cos^2(3\theta) \tag{22}$$

in their augmented void evolution equation. As readily inferred, this yields a symmetric behaviour with respect to generalized shear states corresponding to the Lode parameter $L = 0$ and the deviatoric angle $\theta = 30°$. The simulation data from the unit cell calculations conducted herein imply that the scaling should rather be a monotonically decreasing function with increasing Lode parameter. In particular, the deviatoric scaling function should take a nearly linear form when expressed in terms of the parameter $\cos(3\theta)$, as inferred from Figures 5b, 5d, 5f, and 6b. We note that the relation between $\cos(3\theta)$ and the Lode parameter was given in Equation (5). Following the work of Nahshon and Hutchinson (2008), we use the same general form of $\dot{f}_s$ as in Equation (16). However, as emphasized in Section 2.3, we associate the additional term in Equation (15) with the Lode dependency of the void evolution observed in the unit cell calculations for moderate and high stress triaxialities

rather than shear failure. Instead of the deviatoric scaling function in Equation (22), we propose a linear deviatoric scaling of the form

$$\kappa(\theta) = \frac{1}{2}\left(1 + \cos(3\theta)\right) \tag{23}$$

We note that the notation $\dot{f}_s$ is kept only for convenience in the current exposition, but it may be associated with void *shape* rather than void shearing.

The two different deviatoric scaling functions $\kappa(\theta)$ are depicted in Figure 7 as functions of the Lode parameter, where "NH" refers to Nahshon-Hutchinson and "New" corresponds to the term proposed herein. Note that the non-linear relation between L and $\cos(3\theta)$ in Equation (5) yields the non-linearity of the new scaling function that we observe in the figure. If we embed the new Lode-dependent term into Equation (15), an expression for the void evolution is determined as

$$\dot{f} = (1-f)\,\mathrm{tr}\,(\hat{\mathbf{D}}^{\mathrm{p}}) + \frac{k_s f}{2}\left(1 + \cos(3\theta)\right) D^{\mathrm{p}}_{\mathrm{eq}} \tag{24}$$

Also, note that if the new deviatoric scaling function yields the same response as the one used by Nahshon and Hutchinson (2008) under generalized shear loading, then the shear parameter k_s must be twice as large in the former. The reason for multiplying by $1/2$ in $\kappa(\theta)$ is that we wish to keep the weighting within the range $0 \leq \kappa(\theta) \leq 1$. The parameter k_s will eliminate this difference in practical applications of the model since it then must be appropriately calibrated from experimental data.

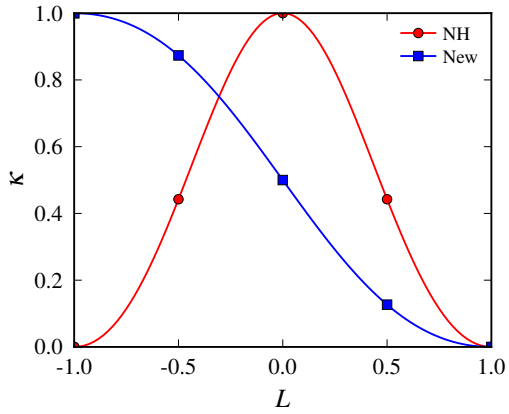

Figure 7: Illustration of the two deviatoric scaling functions used in the shear damage term $\dot{f}_s$. "NH" corresponds to the scaling used by Nahshon and Hutchinson (2008), and "New" refers to the scaling term proposed herein.

5. Model assessment

In this section, we will assess the modified Gurson model. We first compare the model predictions with unit cell calculations under proportional loading paths. Then, we explore some limitations of the model in comparison with unit cell calculations under abrupt non-proportional loading paths. We finally conduct imperfection band analyses to demonstrate the influence of the Lode-dependent void evolution term on ductile failure by strain localization. Note that the assessment of the model undertaken in this section is largely qualitative in the sense that the parameters of the material model are not specifically calibrated.

5.1. Comparisons with unit cell simulations

We compare the predictions of the augmented void evolution law given by Equation (24) based on the notion that the unit cell simulations represent the true material behaviour. We have used the material parameters $f_0 = 0.005$, $q_1 = q_2 = 1$, and $k_s = 0.5$ in the subsequent analyses. No attempt has been made to enhance the

performance of the porous plasticity model by calibrating these material parameters to the unit cell data since our attention is confined to addressing qualitative aspects of the Lode-dependent void evolution governed by Equation (24).

5.1.1. Proportional loading

The predictions of the porous plasticity model with the parameters listed above are compared to the unit cell results in Figure 8 for proportional loading paths governed by a stress triaxiality $T = 1$ and Lode parameters $L = -1, 0, 1$. From these results, we observe that this simple modification of the Gurson model yields a mechanical response that more or less conforms to the unit cell calculations for the shown stress triaxiality ratio. Specifically, the model is able to predict the evolution of the porosity as a function of the equivalent strain for stress states ranging from generalized tension to generalized compression. Note that the other levels of stress triaxiality did not provide predictions that were as good. This result is mainly related to the adopted set of material parameters, and we could easily have found parameter values that are more suitable for a wider range of stress states. Parameter values in the proximity of those proposed by Tvergaard (1982) enhance the performance of the Gurson model in the low and moderate range of stress triaxialities. The q_i parameters have also been the subject of many calibration procedures using unit cell simulations previously reported in the literature (see, e.g. Faleskog et al. (1998) or Dæhli et al. (2017a)), and they generally depend on matrix material properties such as work hardening in addition to the stress states under consideration. In conjunction with the modified void evolution equation, all the material parameters q_1, q_2, and k_s must be determined from some type of experimental data. Since both q_i and k_s affect the mechanical response, they should be calibrated when the extra void evolution term $\dot{f}_s$ is included in the numerical simulations. Nahshon and Hutchinson (2008) found that an appropriate range of values for the shear parameter k_s was $1 \leq k_s \leq 3$. With the current modification of the deviatoric scaling function, there is no guarantee that the same range of parameter values still provides adequate predictions. We do not pursue this issue herein, but it is indeed relevant for future work.

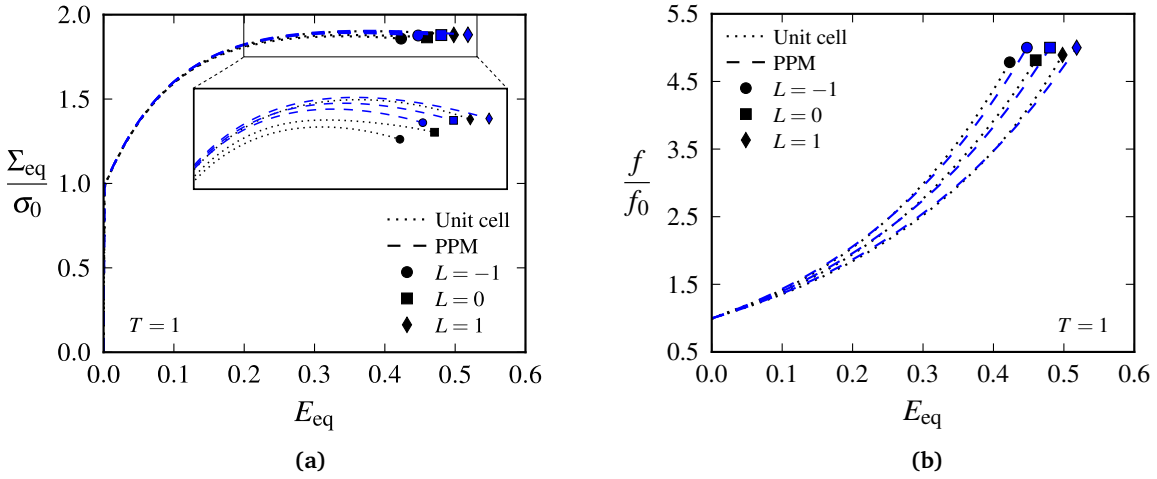

Figure 8: Comparison between the unit cell analyses (black dotted lines) and the porous plasticity model (blue dashed lines) for a stress triaxiality $T = 1$ slightly beyond peak stress. The results pertain to (a) normalized macroscopic stress and (b) normalized porosity evolution. A magnified view of a portion of the stress-strain curve is shown in (a) to aid the comparison.

Since $\dot{f}_s$ scales with the product $\boldsymbol{\Sigma}' : \mathbf{D}^p$, the influence of the Lode-dependent void evolution term fades out for high levels of stress triaxiality and vanishes entirely as $T \to \infty$. Figure 9 clearly shows that the effects of $\dot{f}_s$ have already faded out for a triaxiality ratio $T = 3$ when $k_s = 0.5$. The constant parameter k_s clearly amplifies the contribution from the Lode-dependent term such that the range of triaxiality ratios where $\dot{f}_s$ can be disregarded is generally dependent on the value of k_s. Nonetheless, any effect of $\dot{f}_s$ is considered to be insignificant for rather high stress triaxialities for reasonable values of k_s. This also holds true for the shear-modified Gurson model by Nahshon and Hutchinson (2008). Despite this, Nielsen and Tvergaard (2010) found that the contribution of the

shear damage term was too great for the intermediate triaxiality range in their study of shear failure of spot welds. They further proposed scaling down the shear damage used by Nahshon and Hutchinson (2008) with increasing triaxiality. Such a modification might also be included in the current formulation of the porosity evolution but has not been investigated in this study.

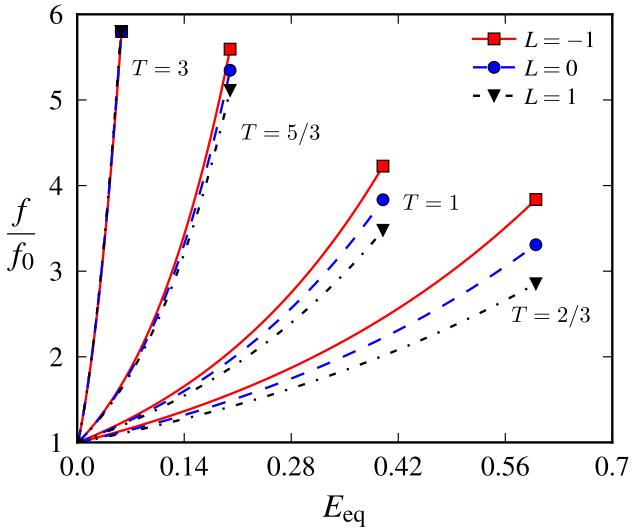

Figure 9: Porosity evolution using the deviatoric scaling function proposed in Equation (23) for various levels of stress triaxiality.

An important limitation of the model must be highlighted. As previously mentioned, the evolution of the porosity from the unit cell simulations shown in Figure 3b indicates that the void tends to collapse when the stress triaxiality is sufficiently low. The voids are more prone to collapse under generalized compression loading, but for some lower stress triaxiality ratios this will also occur for the remaining Lode parameters. Neither the Gurson model nor the heuristic extension presented herein are consistent with this observation since these porous plasticity models invariably predict an increasing porosity for positive stress triaxiality ratios. The physical mechanisms at play are no longer those underpinning the Gurson model, for which void growth is crucial. Such a deficiency requires more refined porous plasticity models that are based on more general void shapes and that account for void rotation (Madou and Leblond, 2012a; Cao et al., 2015).

5.1.2. Non-proportional loading

The loading paths exerted on material elements occupying a material body are rarely proportional, which has important consequences for the evolution of the idealized microstructure and ductile fracture (Benzerga et al., 2012; Basu and Benzerga, 2015; Dæhli et al., 2016; Thomas et al., 2016). A material model should be able to account for the variations in loading path to be predictive. We will now address this issue for both the original Gurson model and the extension proposed in this study by comparing with unit cell calculations. The non-proportional loading paths imposed in these analyses are governed by a step change in either the stress triaxiality (keeping the Lode parameter constant) or the Lode parameter (keeping the stress triaxiality constant). In total, four different loading cases are investigated, which are illustrated in Figures 10a and 10b. The first two loading cases consist of a jump in stress triaxiality (i) $T = 1/3 \rightarrow 1$ or (ii) $T = 1 \rightarrow 1/3$ for generalized tension loading with Lode parameter $L = -1$. The last two loading conditions are governed by a shift in the deviatoric stress state governed by a jump in the Lode parameter (iii) $L = -1 \rightarrow 1$ or (iv) $L = 1 \rightarrow -1$ for the constant stress triaxiality ratio $T = 2/3$. The jump in the stress state is defined to occur approximately at the equivalent strain level for necking in uniaxial tension. Using the material parameters listed in Table 1, the step jump then occurs at an equivalent strain of $E_{\text{eq}} \approx 0.17$. These non-proportional loading paths are chosen rather arbitrarily but represent abrupt changes in the stress state and thus serve to indicate whether the Gurson-based porous plasticity models are able to address such changes in the loading condition.

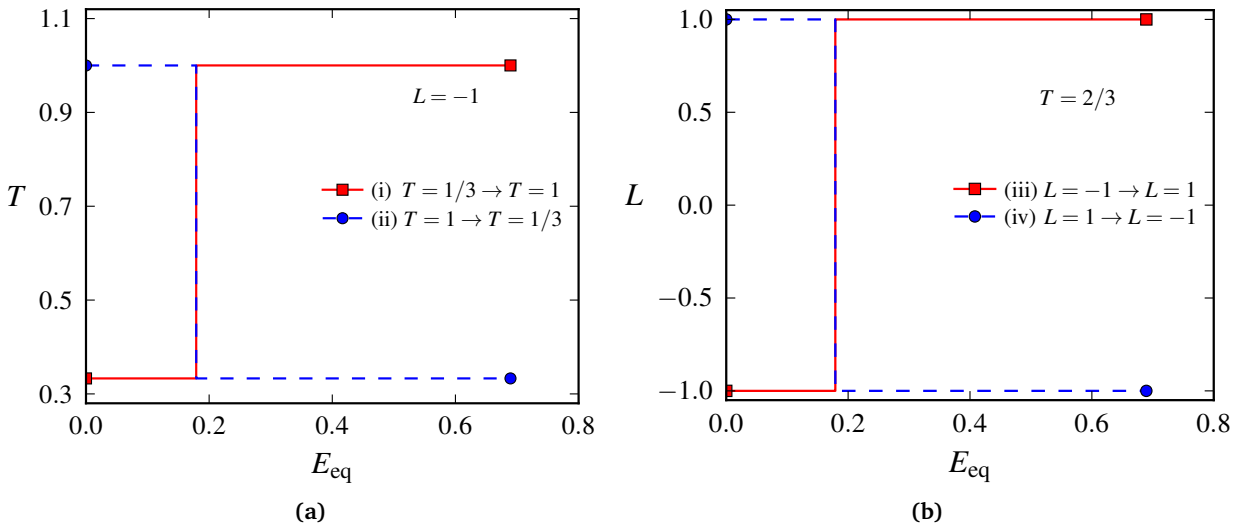

Figure 10: Non-proportional loading paths employed in the analyses. Step jumps in either (a) the stress triaxiality or (b) the Lode parameter are imposed. The step jump is imposed at the equivalent strain level corresponding to necking in uniaxial tension.

Figure 11 shows the normalized porosity evolution for the unit cell model (solid line), the porous plasticity model with the new Lode-dependent void evolution term (dashed line), and the original Gurson model (dotted line). We emphasize that the results should be interpreted on a qualitative basis, since no attempt was made to calibrate the q_i parameters in this study. Considering first loading cases (i) and (ii) shown in Figure 11a, pertaining to a step jump in stress triaxiality, we observe that both porous plasticity models are able to describe a non-proportionality in stress triaxiality. The trends are also qualitatively consistent with the unit cell calculations, which is not surprising considering the strong influence of the stress triaxiality on void growth in the Gurson model (see the first term in Equation (18)). However, for the material parameters employed here, we are not able to obtain accurate predictions for both loading cases using the same set of parameters. This is readily inferred from Figure 11a since the original Gurson model fits rather well for loading case (ii), whereas the Lode-dependent Gurson model yields better predictions for loading case (i). We do not rule out the potential of finding q_i (and k_s for the new extension) such that the Gurson model and its heuristic extension are more accurate for both loading paths, i.e. from low to high (i) and from high to low (ii) stress triaxiality ratios. However, the ability to properly evaluate void growth under high stress triaxiality generally requires q_i parameters (typically $q_1 \approx q_2 \approx 1$) that impair the predictions for lower stress triaxialities, and vice versa. Consequently, for arbitrary non-proportional loading paths, potentially involving low stress triaxiality ratios, this simple extension of the Gurson model is too limited to be fully predictive. Additionally, it is difficult to argue that the new Lode-dependent Gurson model represents an enhancement compared to the original version in the case of a step jump in stress triaxiality, although it would provide some flexibility if stress states with other Lode parameters $L \neq -1$ were used.

The improvements of the Lode-dependent Gurson model compared to the original Gurson model are more apparent if we consider loading cases (iii) and (iv) pertaining to step jumps in the Lode parameter. To this end, let us now turn to the results shown in Figure 11b. From inspection of these curves, the original Gurson model does not exhibit any changes in void growth for a change in the Lode parameter. This follows intuitively from the model formulation being Lode insensitive. The heuristic extension proposed in this work qualitatively exhibits the same behaviour as the unit cell analyses. In this particular case, we are likely to find values for q_i and k_s that provide even better agreement with the unit cell calculations. Consequently, the model possesses some favourable features for full-scale modelling of structural components compared to Gurson's original model (Gurson, 1977).

We finally emphasize that void shape effects are important for strongly non-proportional loading paths. For instance, consider an initially voided unit cell loaded in generalized compression. This promotes an oblate shape (two coinciding major principal radii) in the case of J_2 flow theory. If the unit cell is subsequently loaded in

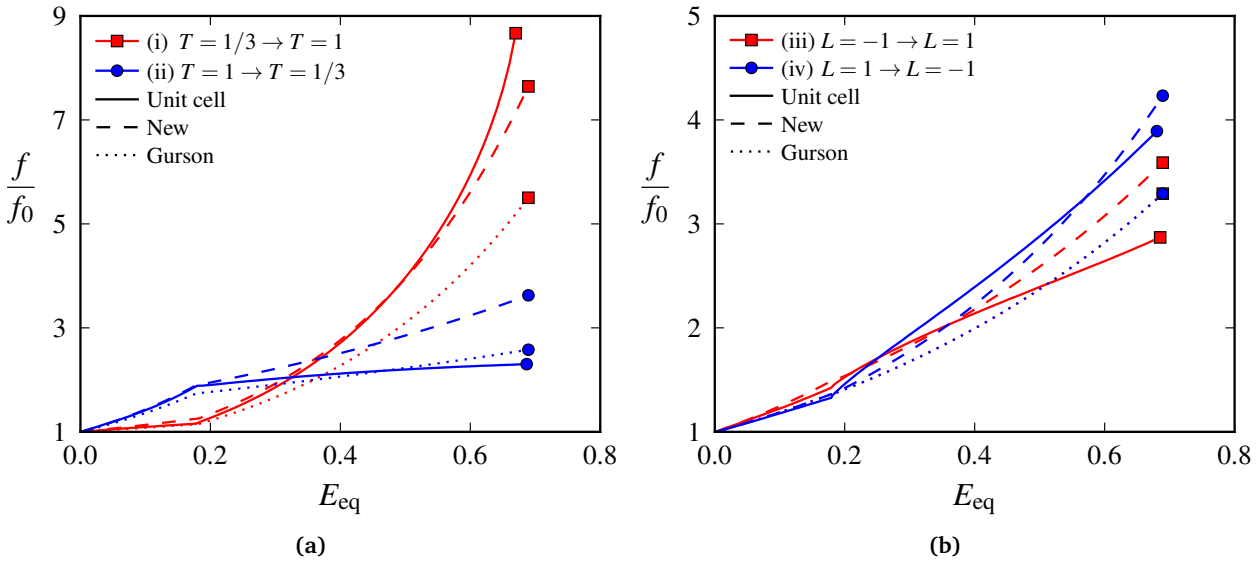

Figure 11: Plots of the normalized porosity evolution obtained with the unit cell (solid lines), the porous plasticity model with the new Lode-dependent term (dashed lines), and the original Gurson model (dotted lined) under non-proportional loading. The loading paths correspond to a step jump in (a) stress triaxiality when the Lode parameter is $L = -1$ and (b) Lode parameter when the stress triaxiality is $T = 2/3$.

generalized tension, with the major principal stress direction normal to the plane spanned by the major principal radii, then it is expected that ductile fracture occurs very rapidly. This is roughly approximated by normal loading of penny-shaped cracks, which is known to be very harmful for the material. However, reloading in generalized tension with the major principal stress direction in the plane spanned by the two major void radii is most likely less detrimental. Although a more complex porous plasticity model with an explicit treatment of the void shape is likely to capture such aspects, the heuristic extension proposed herein will not be able to address this problem. This is related to the fact that the void shape is not explicitly accounted for in the model but only included through the heuristic amplification of the void growth as a function of the deviatoric angle. Consequently, the model cannot sense whether the void is loaded normal to the major principal void radii or along the major principal void radii.

5.2. Strain localization analyses

To examine the effects of the Lode-dependent void evolution term on ductile failure, we use the imperfection band analyses proposed by Rice (1976). Such analyses have previously been employed in the literature to examine strain localization in metals (Needleman and Rice, 1978; Yamamoto, 1978; Saje et al., 1982; Pan et al., 1983; Mear and Hutchinson, 1985; Needleman and Tvergaard, 1992; Morin et al., 2017; Dæhli et al., 2017b) and were also used in the paper by Nahshon and Hutchinson (2008) to examine the effects of their shear-modified Gurson model. In the following, we will construct failure loci based on three-dimensional imperfection band analyses to elucidate the effects of the deviatoric scaling function proposed in this study on the predictions of ductile failure. Ductile failure is in this context associated with strain localization and not void coalescence. Although void coalescence is an important aspect to take into consideration, the imperfection band analyses relax the need for void coalescence criteria because ductile failure in this form often occurs at rather low porosities (see Morin et al. (2017) and Dæhli et al. (2017b)) for moderate and high stress triaxialities. These porosities are generally somewhat lower than the porosity levels at void coalescence evaluated from unit cell simulations. However, detailed studies that account for void coalescence may for instance be found in Pardoen and Hutchinson (2000), Scheyvaerts et al. (2011), and Tekoğlu et al. (2012).

5.2.1. Governing equations and numerical setup

The imperfection band analyses (Rice, 1976) are based on the concept of a homogeneously deforming solid that contains an initial material imperfection in the form of a thin planar band. Material properties, and thus the field quantities, generally deviate between the regions inside and outside the imperfection band. In the following, a brief overview of the main equations will be given under the assumption of an updated Lagrangian description (Mear and Hutchinson, 1985; Nahshon and Hutchinson, 2008; Haddag et al., 2009; Morin et al., 2017). Thus, the reference configuration is taken to momentarily coincide with the current configuration.

Continuing a state of equilibrium across the imperfection band requires that (Rice, 1976)

$$\mathbf{n} \cdot \dot{\mathbf{N}}_\mathrm{b} = \mathbf{n} \cdot \dot{\mathbf{N}}_\mathrm{o} \tag{25}$$

where $\mathbf{n}$ denotes the band normal in the updated reference configuration. The nominal stress rates $\dot{\mathbf{N}}_\mathrm{b}$ and $\dot{\mathbf{N}}_\mathrm{o}$ are those obtained inside and outside the imperfection band, respectively. Compatibility requirements further imply that the difference in the velocity gradient fields inside and outside the imperfection are related through

$$\mathbf{L}_\mathrm{b} = \mathbf{L}_\mathrm{o} + \dot{\mathbf{q}} \otimes \mathbf{n} \tag{26}$$

Here, $\mathbf{L}_\mathrm{b}$ and $\mathbf{L}_\mathrm{o}$ are the velocity gradient tensors inside and outside the band, respectively, while $\dot{\mathbf{q}}$ denotes the non-uniformity across the imperfection band.

The rate constitutive equations inside and outside the band are written quite generally as

$$\dot{\mathbf{N}}_\mathrm{b} = \mathbf{C}^\mathrm{t}_\mathrm{b} : \mathbf{L}_\mathrm{b} \tag{27a}$$

$$\dot{\mathbf{N}}_\mathrm{o} = \mathbf{C}^\mathrm{t}_\mathrm{o} : \mathbf{L}_\mathrm{o} \tag{27b}$$

where the tangent stiffness $\mathbf{C}^\mathrm{t}$ contains both the material tangent stiffness and terms that emerge in large deformation theory. By combination of Equations (25), (26), (27a), and (27b), an equation for the non-uniformity $\dot{\mathbf{q}}$ is obtained as

$$\left(\mathbf{n} \cdot \mathbf{C}^\mathrm{t}_\mathrm{b} \cdot \mathbf{n}\right) \cdot \dot{\mathbf{q}} = \mathbf{n} \cdot \left(\mathbf{C}^\mathrm{t}_\mathrm{o} - \mathbf{C}^\mathrm{t}_\mathrm{b}\right) : \mathbf{L}_\mathrm{o} \tag{28}$$

Strain localization is determined from the instant when the determinant of the acoustic tensor becomes singular, viz.

$$\det\left(\mathbf{n} \cdot \mathbf{C}^\mathrm{t}_\mathrm{b} \cdot \mathbf{n}\right) = 0 \tag{29}$$

This corresponds to loss of ellipticity of the governing equations inside the imperfection band. In the current exposition, the material outside the imperfection band is simply represented by J_2 flow theory, while the material inside the imperfection band is governed by either (i) the original Gurson model (Gurson, 1977), (ii) the shear-modified Gurson model (Nahshon and Hutchinson, 2008), or (iii) the Lode-dependent Gurson model proposed in Section 4.2. The porous plasticity parameters used in the following correspond to $f_0 = 0.005$, $q_1 = q_2 = 1$, and $k_\mathrm{s} = 1$.

5.2.2. Results

We conducted imperfection band analyses under prescribed proportional loading paths. To this end, levels of stress triaxiality and Lode parameter are assigned to the homogeneously deforming material outside the band. However, the loading paths exerted on the material inside the imperfection band are generally non-proportional and may deviate quite substantially from the macroscopically proportional loading due to the simultaneous fulfilment of equilibrium and compatibility. In fact, this is a key feature of the imperfection band analyses that gives rise to differences in the failure strain under generalized tension and generalized compression even with the original Lode-insensitive Gurson model (Morin et al., 2017).

The failure strains are depicted in Figures 12a-12d against the Lode parameter for the stress triaxialities $T = 2/3$, 1, $5/3$, and 3, respectively. Failure loci obtained using the original Gurson model inside the imperfection band are indicated by the black solid lines with circle markers. The failure strain levels using the model of Nahshon and Hutchinson (2008) are referred to as NH and shown with red solid lines and square markers. Furthermore, the results using the Lode-dependent void evolution term proposed herein are indicated using blue solid lines and

diamond markers.

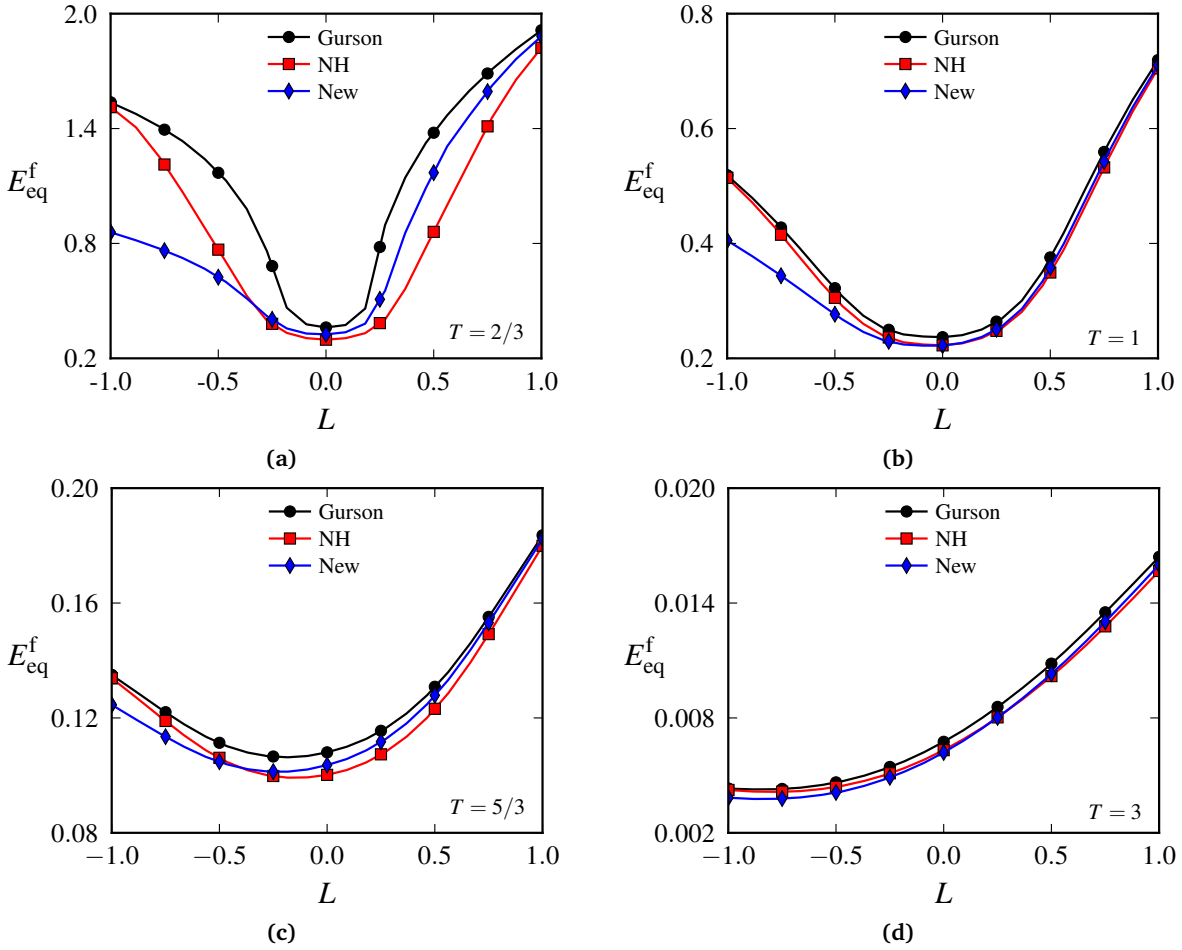

Figure 12: Failure loci generated from imperfection band analyses showing the effect of using different void evolution equations in the band material. The results for the original Gurson model, the shear-modified Gurson model by Nahshon and Hutchinson (NH), and the shear modification proposed herein (New) are compared. The figures pertain to stress triaxialities (a) $T = 2/3$, (b) $T = 1$, (c) $T = 5/3$, and (d) $T = 3$ and span the range of admissible Lode parameters.

Since the damage term $\dot{f}_{\mathrm{s}}$ can only participate in accelerating the void growth, the failure loci for the original Gurson always define the upper limit to the failure strain. In the case of the two lowest stress triaxialities $T = 2/3$ and 1, we find a prominent effect of the additional porosity evolution term $\dot{f}_{\mathrm{s}}$ with both the deviatoric scaling function from Nahshon and Hutchinson (2008) and the one proposed herein. The major differences between the three models are found for generalized tension loading. Due to the deviatoric scaling used in Equation (23), the failure strain is much lower for the void evolution equation proposed in this study. Under these circumstances, the deviatoric scaling function in Equation (22) used by Nahshon and Hutchinson (2008) reduces to zero. Consequently, the failure strain prediction is very close to the original Gurson model, with the difference being related to the drift of the stress state inside the imperfection band triggering some effects of $\dot{f}_{\mathrm{s}}$. The same observation applies to the case of generalized compressive loading, in which the Lode-dependent scaling terms in Equation (22) and Equation (23) reduce to zero and the ductility predictions of all three models are close to identical. Although the generalized shear states yield the lowest failure strain values for the two lower stress triaxialities, there are only minor differences between the predictions using the various void evolution laws for $L = 0$. This difference can easily be amplified by changing the value for k_{s}. However, we note that this will affect the entire failure locus, and the effects of changing k_{s} are considered to be most prominent in the generalized

tension loading range.

The discrepancies between the failure loci obtained with the three different void evolution equations become small as the triaxiality ratio is increased. In these circumstances, the major contribution stems from the original void growth term related to the volumetric plastic strain rate $\dot{f}_g$. Thus, as T increases, $\dot{f}_g$ will dominate in favour of $\dot{f}_s$ and the failure strain levels using either of the three models tend to conform. This result is generally dependent on the material parameters employed in the porous plasticity model. However, under purely hydrostatic stress states, the increase in the void volume fraction should only be related to $\dot{f}_g$ since the original Gurson model represents the exact solution in this case. This will be satisfied because $\dot{f}_s$ is linked to the product $\hat{\boldsymbol{\Sigma}}' : \hat{\mathbf{D}}$, which has already been discussed in Section 5.1 and demonstrated in Figure 9.

The main difference between the shear damage term by Nahshon and Hutchinson (2008) and the Lode-dependent void evolution term proposed herein in terms of strain localization analyses is related to the skewness of the resulting failure locus. Although both the original Gurson model and the shear-modified Gurson model display a skewed failure locus, the effect of the Lode parameter is more pronounced for the new Lode-dependent void evolution term. Although a proper calibration of the porous plasticity models to unit cell calculations is not presented here, we note that the shape of the failure loci of the proposed model is in better qualitative agreement with those obtained using detailed unit cell simulations (Barsoum and Faleskog, 2011; Dunand and Mohr, 2014; Wong and Guo, 2015) that resembles the imperfection band analyses. Such unit cell analyses typically exhibit a drastic increase in ductility under generalized compression loading, which renders failure loci more consistent with those of the new model shown in Figure 12.

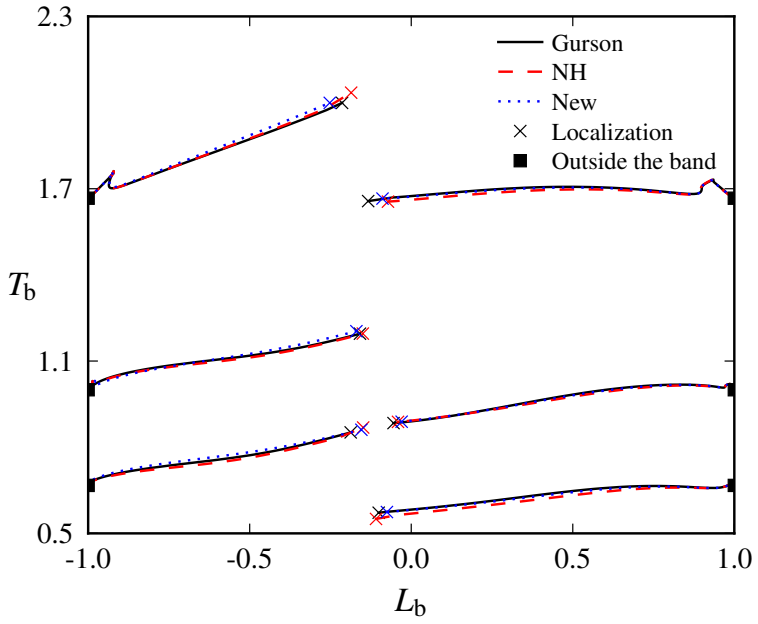

Figure 13: Evolution of the stress state in terms of the stress triaxiality and Lode parameter inside the imperfection band (T_b, L_b). The stress states prescribed outside the imperfection correspond to either generalized tension $L = -1$ or generalized compression $L = 1$. Points marked by "×" denote the onset of strain localization, while those marked by "■" denote the homogeneous stress state outside the band.

The mechanical field quantities inside the imperfection band substantially deviate from those outside the band. This is readily observed from the curves plotted in Figure 13, which show the stress triaxiality T_b as a function of the Lode parameter L_b inside the imperfection band. The displayed curves pertain to either stress states of generalized tension ($L = -1$) or generalized compression ($L = 1$) imposed to the homogeneously deformed material outside the imperfection band. One finding of particular interest is that in the case of generalized compression, the triaxiality ratio inside the imperfection band decreases from its initially imposed value. The

opposite holds true for generalized tension, which causes the skew failure loci in the case of the original Gurson model and the shear-modified Gurson model. However, with the Lode-dependent void evolution term proposed in this study, the accumulation of damage is by itself non-symmetric with respect to generalized shear. This Lode-dependency of the damage accumulation adds to the drift of the stress state inside the imperfection band and causes an even greater skewness of the failure loci. The influence of this combined effect is readily inferred from Figures 12a and 12b. We note that the drift from the homogeneous stress state outside the band is the only reason for the small discrepancy observed between the three models in the case of generalized compressive loading ($L = 1$), and it is also the reason for the difference between the models of Gurson (1977) and Nahshon and Hutchinson (2008) in the case of generalized tension loading ($L = -1$).

6. Concluding remarks

Numerical analyses of an idealized microstructure for a porous ductile solid show that the void growth is dependent on the deviatoric stress state. A modification of the Gurson porous plasticity model is proposed to better capture the porosity evolution observed in these unit cell calculations. The unit cell simulations are conducted under moderate and high stress triaxiality ratios without the effects of void rotation due to shearing, but an additional set of calculations was also performed for a zero triaxiality ratio using a rigid particle in the unit cell. These simulations suggest that an appropriate weighting of the void growth with the deviatoric stress state can be defined by a linear relation in terms of $\cos(3\theta)$. This extension of the Gurson model is examined herein by assessments using unit cell calculations and strain localization analyses. First, direct comparisons of the performance of the porous plasticity model are performed with data from unit cell simulations under the application of both proportional and non-proportional loading paths. Next, the predictions of ductile failure by the use of imperfection band analyses are compared using the original Gurson model, the shear-modified Gurson model, and the Lode-dependent Gurson model proposed herein. By inspecting the resulting failure loci, we find a marked decrease in ductility under predominant generalized tension loading. Furthermore, the failure loci obtained with the Lode-dependent void evolution term proposed in this study are more consistent with the Gurson model in the range of generalized compression, where the effect of the augmented damage term drops off faster than in the model by Nahshon and Hutchinson (2008). In effect, the new Lode-dependent void evolution term leads to a greater difference between the ductility limits in generalized tension and generalized compression. This behaviour is in better agreement with more elaborate unit cell calculations where the imperfection band material is explicitly modelled.

Based on the numerical observations in this study, we believe that such an extension of the Gurson model is relevant for structural analyses where ductile failure should be included in the constitutive framework. However, we have only performed comparisons with the evolution of a highly idealized material microstructure and have not conducted any assessments of the model that are in line with typical engineering applications. Consequently, we note that the Lode-dependent void evolution equation must be properly validated before it can be employed in large-scale simulations of structural components. We also emphasize that this extension of the Gurson model is motivated by the evolution of an idealized material microstructure under moderate and high levels of macroscopic stress triaxiality. In this range of stress states, the predictive capabilities of the model are considered to be adequate since the model reflects the findings from the unit cell simulations. However, the model is less accurate in the case of lower stress triaxialities. Under such conditions, the physical processes leading to ductile fracture are not consistent with the assumptions underpinning the Gurson model and the heuristic extension presented in this study.

Acknowledgements

The financial support of this work from the Centre for Advanced Structural Analysis (CASA), Centre for Research-based Innovation (CRI), at the Norwegian University of Science and Technology (NTNU) and the Research Council of Norway through project no. 237885 (CASA) is gratefully acknowledged.

References

Abaqus, 2013. Version 6.13. Dassault Systèmes Simulia Corp., Providence, RI, USA.

Bao, Y., Wierzbicki, T., 2004. On fracture locus in the equivalent strain and stress triaxiality space. International Journal of Mechanical Sciences 46, 81–98.

Barsoum, I., Faleskog, J., 2007. Rupture mechanisms in combined tension and shear-Experiments. International Journal of Solids and Structures 44, 1768–1786.

Barsoum, I., Faleskog, J., 2011. Micromechanical analysis on the influence of the Lode parameter on void growth and coalescence. International Journal of Solids and Structures 48, 925–938.

Basu, S., Benzerga, A. A., 2015. On the path-dependence of the fracture locus in ductile materials: Experiments. International Journal of Solids and Structures 71, 79–90.

Beese, A. M., Luo, M., Li, Y., Bai, Y., Wierzbicki, T., 2010. Partially coupled anisotropic fracture model for aluminum sheets. Engineering Fracture Mechanics 77 (7), 1128–1152.

Benzerga, A. A., Surovik, D., Keralavarma, S. M., 2012. On the path-dependence of the fracture locus in ductile materials - Analysis. International Journal of Plasticity 37, 157–170.

Brünig, M., Gerke, S., Hagenbrock, V., 2013. Micro-mechanical studies on the effect of the stress triaxiality and the Lode parameter on ductile damage. International Journal of Plasticity 50, 49–65.

Budiansky, B., Hutchinson, J. W., Slutsky, S., 1982. Void growth and collapse in viscous solids. In: Mechanics of Solids: The Rodney Hill 60th Anniversary Volume. Pergamon Press, London, pp. 13–46.

Cao, T., Mazière, M., Danas, K., Besson, J., 2015. A model for ductile damage prediction at low stress triaxialities incorporating void shape change and void rotation. International Journal of Solids and Structures 63, 240–263.

Cheng, L., Guo, T., 2007. Void interaction and coalescence in polymeric materials. International Journal of Solids and Structures 44 (6), 1787–1808.

Dæhli, L. E. B., Børvik, T., Hopperstad, O. S., 2016. Influence of loading path on ductile fracture of tensile specimens made from aluminium alloys. International Journal of Solids and Structures 88-89, 17–34.

Dæhli, L. E. B., Faleskog, J., Børvik, T., Hopperstad, O. S., 2017a. Unit cell simulations and porous plasticity modelling for strongly anisotropic FCC metals. European Journal of Mechanics A/Solids 65, 360–383.

Dæhli, L. E. B., Morin, D., Børvik, T., Hopperstad, O. S., 2017b. Influence of yield surface curvature on the macroscopic yielding and ductile failure of isotropic porous plastic materials. Journal of the Mechanics and Physics of Solids 107, 253–283.

Dunand, M., Mohr, D., 2014. Effect of Lode parameter on plastic flow localization after proportional loading at low stress triaxialities. Journal of the Mechanics and Physics of Solids 66 (1), 133–153.

Faleskog, J., Barsoum, I., 2013. Tension-torsion fracture experiments - Part I: Experiments and a procedure to evaluate the equivalent plastic strain. International Journal of Solids and Structures 50, 4241–4257.

Faleskog, J., Gao, X., Shih, C. F., 1998. Cell model for nonlinear fracture analysis – I. Micromechanics calibration. International Journal of Fracture 89, 355–373.

Gao, X., Kim, J., 2006. Modeling of ductile fracture: Significance of void coalescence. International Journal of Solids and Structures 43, 6277–6293.

Gologanu, M., Leblond, J. B., Devaux, J., 1993. Approximate models for ductile metals containing non-spherical voids – Case of axisymmetric prolate ellipsoidal cavities. Journal of the Mechanics and Physics of Solids 41, 1723–1754.

Gologanu, M., Leblond, J.-B., Devaux, J., 1994. Approximate Models for Ductile Metals Containing Nonspherical Voids - Case of Axisymmetric Oblate Ellipsoidal Cavities. Journal of Engineering Materials and Technology 116, 290–297.

Gurson, A. L., 1977. Continuum Theory of Ductile Rupture by Void Nucelation and Growth: Part I – Yield Criteria and Flow Rules for Porous Ductile Media. Journal of Engineering Materials and Technology 99, 2—-15.

Haddag, B., Abed-Meraim, F., Balan, T., 2009. Strain localization analysis using a large deformation anisotropic elastic-plastic model coupled with damage. International Journal of Plasticity 25, 1970–1996.

Haltom, S. S., Kyriakides, S., Ravi-Chandar, K., 2013. Ductile failure under combined shear and tension. International Journal of Solids and Structures 50, 1507–1522.

Kim, J., Gao, X., Srivatsan, T. S., 2004. Modeling of void growth in ductile solids: Effects of stress triaxiality and initial porosity. Engineering Fracture Mechanics 71, 379–400.

Korbel, A., Raghunathan, V. S., Teirlinck, D., Spitzig, W., Richmond, O., Embury, J. D., 1984. A structural study of the influence of pressure on shear band formation. Acta Metallurgica 32 (4), 511–519.

Liu, Z. G., Wong, W. H., Guo, T. F., 2016. Void behaviors from low to high triaxialities: Transition from void collapse to void coalescence. International Journal of Plasticity 84, 183–202.

Madou, K., Leblond, J. B., 2012a. A Gurson-type criterion for porous ductile solids containing arbitrary ellipsoidal voids - I: Limit-analysis of some representative cell. Journal of the Mechanics and Physics of Solids 60, 1020–1036.

Madou, K., Leblond, J. B., 2012b. A Gurson-type criterion for porous ductile solids containing arbitrary ellipsoidal voids - II: Determination of yield criterion parameters. Journal of the Mechanics and Physics of Solids 60, 1037–1058.

Mear, M. E., Hutchinson, J. W., 1985. Influence of yield surface curvature on flow localization in dilatant plasticity. Mechanics of Materials 4, 395–407.

Morin, D., Hopperstad, O. S., Benallal, A., 2017. On the description of ductile fracture in metals by the strain localization theory. International Journal of Fracture.

Nahshon, K., Hutchinson, J. W., 2008. Modification of the Gurson Model for shear failure. European Journal of Mechanics - A/Solids 27, 1–17.

Needleman, A., Rice, J., 1978. Limits to ductililty set by plastic flow localization. Mechanics of Sheet Metal Forming, 237 —- 265.

Needleman, A., Tvergaard, V., 1992. Analyses of Plastic Flow Localization in Metals. Applied Mechanics Reviews 45 (3), S3.

Nielsen, K. L., Tvergaard, V., 2010. Ductile shear failure or plug failure of spot welds modelled by modified Gurson model. Engineering Fracture Mechanics 77, 1031–1047.
Pan, J., Saje, M., Needleman, A., 1983. Localization of deformation in rate sensitive porous plastic solids. International Journal of Fracture 21, 261–278.
Papasidero, J., Doquet, V., Mohr, D., 2015. Ductile fracture of aluminum 2024-T351 under proportional and non-proportional multi-axial loading: BaoâĂŞWierzbicki results revisited. International Journal of Solids and Structures 69-70, 459–474.
Pardoen, T., Hutchinson, J. W., 2000. Extended model for void growth and coalescence. Journal of the Mechanics and Physics of Solids 48, 2467–2512.
Rice, J. R., 1976. The Localization of Plastic Deformation. Proceedings of the 14th International Congress on Theoretical and Applied Mechanics 1, 207–220.
Saje, M., Pan, J., Needleman, A., 1982. Void nucleation effects on shear localization in porous plastic solids. International Journal of Fracture 19, 163–182.
Scales, M., Tardif, N., Kyriakides, S., 2016. Ductile failure of aluminum alloy tubes under combined torsion and tension. International Journal of Solids and Structures 97-98, 116–128.
Scheyvaerts, F., Onck, P. R., Tekoğlu, C., Pardoen, T., 2011. The growth and coalescence of ellipsoidal voids in plane strain under combined shear and tension. Journal of the Mechanics and Physics of Solids 59, 373–397.
Teirlinck, D., Zok, F., Embury, J. D., Ashby, M. F., 1988. Fracture mechanism maps in stress space. Acta Metallurgica 36 (5), 1213–1228.
Tekoğlu, C., Leblond, J.-B., Pardoen, T., 2012. A criterion for the onset of void coalescence under combined tension and shear. Journal of the Mechanics and Physics of Solids 60, 1363–1381.
Thomas, N., Basu, S., Benzerga, A. A., 2016. On fracture loci of ductile materials under non-proportional loading. International Journal of Mechanical Sciences 117, 135–151.
Tvergaard, V., 1981. Influence of voids on shear band instabilities under plane strain conditions. International Journal of Fracture 17, 389–407.
Tvergaard, V., 1982. On localization in ductile materials containing spherical voids. International Journal of Fracture 18, 237–252.
Vadillo, G., Reboul, J., Fernández-Sáez, J., 2016. A modified Gurson model to account for the influence of the Lode parameter at high triaxialities. European Journal of Mechanics, A/Solids 56, 31–44.
Westermann, I., Pedersen, K. O., Furu, T., Børvik, T., Hopperstad, O. S., 2014. Effects of particles and solutes on strength, work-hardening and ductile fracture of aluminium alloys. Mechanics of Materials 79, 58–72.
Wong, W. H., Guo, T. F., 2015. On the energetics of tensile and shear void coalescences. Journal of the Mechanics and Physics of Solids 82, 259–286.
Xue, L., 2008. Constitutive modeling of void shearing effect in ductile fracture of porous materials. Engineering Fracture Mechanics 75, 3343–3366.
Yamamoto, H., 1978. Conditions for shear localization in the ductile fracture of void-containing materials. International Journal of Fracture 14, 347–365.
Zhang, K., Bai, J. B., François, D., 2001. Numerical analysis of the influence of the Lode parameter on void growth. International Journal of Solids and Structures 38, 5847–5856.
Zhou, J., Gao, X., Sobotka, J. C., Webler, B. A., Cockeram, B. V., 2014. On the extension of the Gurson-type porous plasticity models for prediction of ductile fracture under shear-dominated conditions. International Journal of Solids and Structures 51, 3273–3291.